Computer Methods in Applied Mechanics and Engineering 417 (2023) 116452

Contents lists available at ScienceDirect

Comput. Methods Appl. Mech. Engrg.

journal homepage: www.elsevier.com/locate/cma

An *hp* error analysis of a hybrid discontinuous mixed Galerkin method for linear viscoelasticity☆

Salim Meddahi

Facultad de Ciencias, Universidad de Oviedo, Federico García Lorca, 18, 33007 Oviedo, Spain

ARTICLE INFO

MSC:
65M30
65M12
65M15
74H15

Keywords:
Hybrid discontinuous Galerkin method
Linear viscoelasticity
Stress-based formulation
Error estimates

ABSTRACT

We present a hybrid discontinuous Galerkin method for the velocity/stress formulation of Zener's model in dynamic viscoelasticity. Our approach utilizes a spatial discretization that enforces strongly the symmetry of the stress tensor, and that allows for efficient handling of heterogeneous materials comprising both purely elastic and viscoelastic components. We provide an *hp* error analysis of the semidiscrete scheme, which yields quasi-optimal error estimates for the stress tensor and sub-optimal error estimates for the velocity field in the L^2-norm. Next, we apply the Crank–Nicolson rule as a time-stepping scheme and analyze its primary convergence properties. Finally, we present the results of numerical experiments to validate our approach and confirm the theoretical rates of convergence.

1. Introduction

Viscoelasticity is the property exhibited by certain materials like biological tissues, elastomers, and polymers, which demonstrate both elastic and viscous behavior. The characteristic of viscoelasticity plays a crucial role in designing products that require features like flexibility, durability, and resistance to deformation. Additionally, it finds extensive usage in applications that need noise control, vibration attenuation, and shock absorption. The viscoelastic problem we are examining in this article draws from Zener's model [1], commonly referred to as the standard model. It is known for being the simplest approach that replicates fundamental viscoelastic behaviors like stress-relaxation and creep-recovery [2].

In the traditional approach to the mathematical and numerical study of viscoelasticity, the problem is formulated solely in terms of the displacement field, which leads to a weak formulation that is non-local in time [3,4]. Recently, formulations that prioritize the stress tensor as the primary unknown have emerged [5–10]. This mixed finite element approach has several advantages, including yielding purely differential variational formulations and providing a direct and accurate approximation of stress, which is a critical quantity in many applications. Additionally, it is well-known that stress-based formulations of the elasticity system are immune to locking phenomena in the nearly incompressible case [11].

However, mixed finite elements for linear elasticity also present several challenges, such as the preservation of the Cauchy stress symmetry. This symmetry guarantees the conservation of angular momentum, and achieving it exactly with conforming finite elements requires a large number of degrees of freedom, see [12,13] and the references therein. To address this issue, one can relax this constraint by imposing it weakly through a variational equation [14]. This method has been successfully adopted for viscoelasticity in [6–9]. Alternatively, nonconforming or DG methods can be used to strongly impose the symmetry of the stress tensor at the discrete level [15–19]. This approach has been recently explored in [10] for the standard model of viscoelasticity.

☆ This research was supported by Ministerio de Ciencia e Innovación, Spain, Project PID2020-116287GB-I00.
E-mail address: salim@uniovi.es.

https://doi.org/10.1016/j.cma.2023.116452
Received 1 July 2023; Received in revised form 18 August 2023; Accepted 11 September 2023
Available online 25 September 2023

Regardless of the approach taken, dealing with tensorial unknowns requires significant computational effort, especially in viscoelasticity where the global stress variable $\boldsymbol{\sigma}$ is represented by two tensors [5]: the elastic component $\boldsymbol{\sigma}_E$ and the viscoelastic component $\omega\boldsymbol{\sigma}_V$, with $\boldsymbol{\sigma} = \boldsymbol{\sigma}_E + \omega\boldsymbol{\sigma}_V$. The scalar parameter ω represents the characteristic relaxation time, which indicates the time for the stress to decay to zero under constant-strain conditions.

An efficient technique to reduce the significant computational effort involved in the mixed finite element approximation of viscoelasticity is to employ the Fraeijs de Veubeke hybridization strategy [11], as suggested in [7]. This hybrid mixed method is further improved in [9] by releasing the discrete elastic and viscoelastic components of the stress from any continuity condition and only requiring their sum $\boldsymbol{\sigma}$ to be H(div)-conforming. Using this approach, the number of degrees of freedom is halved at each implicit time iteration step when compared to [7].

The Discontinuous Galerkin (DG) method introduced in [10] for viscoelasticity enjoys the desirable properties of DG methods such as *hp*-adaptivity, arbitrary order approximations, local conservation, and flexibility in mesh design. However, despite the reduction in unknowns resulting from the strong imposition of stress symmetry, this method still suffers from the typical proliferation of degrees of freedom that DG methods tend to produce in comparison to conforming finite element methods.

In this work, we address this concern by introducing a hybridizable discontinuous Galerkin (HDG) method for viscoelasticity, which combines the advantages of DG methods and hybridization techniques. The general concepts behind the hybridization of DG methods are detailed in [20,21] for different boundary value problems, and its application to the elasticity system is discussed in [22–25]. Essentially, the hybridization procedure reduces the number of globally coupled degrees of freedom by enforcing inter-element continuity through additional traces. This feature enables the method to be implemented efficiently using static condensation [26]. It also facilitates parallelization [27,28], which makes it even more attractive for computationally demanding problems.

We present a new HDG space discretization method for the stress/velocity formulation of Zener's viscoelasticity model. The method utilizes symmetric tensors with piecewise polynomial entries of arbitrary degree $k \geq 0$ to approximate each stress component in both 2D and 3D. Additionally, the discrete velocity field and the discrete trace variable defined on the mesh skeleton are piecewise polynomials of degree $k+1$. We provide an *hp*-version finite element analysis of this mixed HDG semi-discrete scheme. The stability of the scheme is proven with respect to the discretization parameters h and k, as well as with respect to the relaxation time ω, which is assumed to be piecewise constant. This allows for the possibility of composite elastic-viscoelastic structures when ω vanishes in certain areas of the domain. Under piecewise regularity assumptions on the exact solution of the problem, we obtain *hp* error estimates in the L^2-norms for the stress and velocity. The convergence rate for the stress variable is quasi-optimal with respect to the mesh size h, but only suboptimal by half a power with respect to the polynomial degree k. On the other hand, the *hp* error estimate for the velocity is suboptimal by one power in h, which has been confirmed by numerical results. Additionally, we prove that the fully discrete scheme relying on the classical second-order implicit Crank–Nicolson method is stable and convergent.

The plan of the paper is as follows. In the remainder of this section, we provide preliminary notational conventions and define the functional spaces employed in this article. Zener's model for linear viscoelasticity is introduced in Section 2, along with its stress/velocity weak formulation, and the results on its unique solvability are reviewed. In Section 3, we compile preliminary definitions and utilize well-known local *hp* approximation estimates to obtain the global approximation estimates required for our analysis. The definition of the semi-discrete mixed HDG method and its *hp* convergence analysis are detailed in Section 4, and the fully discrete case is treated in Section 5. Finally, several numerical results are presented in Section 6, confirming the expected rates of convergence for different parameter sets including the nearly incompressible regime.

Recurrent notation and Sobolev spaces. We denote the space of real matrices of order $d \times d$ by $\mathbb{M}$, and let $\mathbb{S} := \{\boldsymbol{\tau} \in \mathbb{M};\ \boldsymbol{\tau} = \boldsymbol{\tau}^{\mathrm{t}}\}$ be the subspace of symmetric matrices, where $\boldsymbol{\tau}^{\mathrm{t}} := (\tau_{ji})$ stands for the transpose of $\boldsymbol{\tau} = (\tau_{ij})$. The component-wise inner product of two matrices $\boldsymbol{\sigma}, \boldsymbol{\tau} \in \mathbb{M}$ is defined by $\boldsymbol{\sigma} : \boldsymbol{\tau} := \sum_{i,j} \sigma_{ij}\tau_{ij}$.

Let D be a polyhedral Lipschitz bounded domain of $\mathbb{R}^d$ $(d = 2, 3)$, with boundary ∂D. Along this paper we apply all differential operators row-wise. Hence, given a tensorial function $\boldsymbol{\sigma} : D \to \mathbb{M}$ and a vector field $\boldsymbol{u} : D \to \mathbb{R}^d$, we set the divergence $\mathbf{div}\,\boldsymbol{\sigma} : D \to \mathbb{R}^d$, the gradient $\boldsymbol{\nabla u} : D \to \mathbb{M}$, and the linearized strain tensor $\boldsymbol{\varepsilon}(\boldsymbol{u}) : \Omega \to \mathbb{S}$ as

$$(\mathbf{div}\,\boldsymbol{\sigma})_i := \sum_j \partial_j \sigma_{ij}, \quad (\boldsymbol{\nabla u})_{ij} := \partial_j u_i, \quad \text{and} \quad \boldsymbol{\varepsilon}(\boldsymbol{u}) := \frac{1}{2}\left[\boldsymbol{\nabla u} + (\boldsymbol{\nabla u})^{\mathrm{t}}\right].$$

For $s \in \mathbb{R}$, $H^s(D, E)$ stands for the usual Hilbertian Sobolev space of functions with domain D and values in E, where E is either $\mathbb{R}$, $\mathbb{R}^d$ or $\mathbb{S}$. In the case $E = \mathbb{R}$ we simply write $H^s(D)$. The norm of $H^s(D, E)$ is denoted $\|\cdot\|_{s,D}$ and the corresponding semi-norm $|\cdot|_{s,D}$, indistinctly for $E = \mathbb{R}, \mathbb{R}^d, \mathbb{S}$. We use the convention $H^0(D, E) := L^2(D, E)$ and let $(\cdot,\cdot)_D$ be the inner product in $L^2(D, E)$, for $E = \mathbb{R}, \mathbb{R}^d, \mathbb{S}$, namely,

$$(\boldsymbol{u}, \boldsymbol{v})_D := \int_D \boldsymbol{u} \cdot \boldsymbol{v},\ \forall \boldsymbol{u}, \boldsymbol{v} \in L^2(D, \mathbb{R}^d), \quad (\boldsymbol{\sigma}, \boldsymbol{\tau})_D := \int_D \boldsymbol{\sigma} : \boldsymbol{\tau},\ \forall \boldsymbol{\sigma}, \boldsymbol{\tau} \in L^2(D, \mathbb{S}). \tag{1.1}$$

The space of tensors in $L^2(D, \mathbb{S})$ with divergence in $L^2(D, \mathbb{R}^d)$ is denoted $H(\mathbf{div}, D, \mathbb{S})$. The corresponding norm is given by $\|\boldsymbol{\tau}\|^2_{H(\mathbf{div},D)} := \|\boldsymbol{\tau}\|^2_{0,D} + \|\mathbf{div}\,\boldsymbol{\tau}\|^2_{0,D}$. Let $\boldsymbol{n}$ be the outward unit normal vector to ∂D, the Green formula

$$(\boldsymbol{\tau}, \boldsymbol{\varepsilon}(\boldsymbol{v}))_D + (\mathbf{div}\,\boldsymbol{\tau}, \boldsymbol{v})_D = \int_{\partial D} \boldsymbol{\tau}\boldsymbol{n} \cdot \boldsymbol{v} \qquad \forall \boldsymbol{v} \in H^1(D, \mathbb{R}^d), \tag{1.2}$$

can be used to extend the normal trace operator $\boldsymbol{\tau} \to (\boldsymbol{\tau}|_{\partial D})\boldsymbol{n}$ to a linear continuous mapping $(\cdot|_{\partial D})\boldsymbol{n} : H(\mathbf{div}, D, \mathbb{S}) \to H^{-\frac{1}{2}}(\partial D, \mathbb{R}^d)$, where $H^{-\frac{1}{2}}(\partial D, \mathbb{R}^d)$ is the dual of $H^{\frac{1}{2}}(\partial D, \mathbb{R}^d)$.

Sobolev spaces for time dependent problems. Since we will deal with a space–time domain problem, besides the Sobolev spaces defined above, we need to introduce spaces of functions acting on a bounded time interval $(0, T)$ and with values in a separable

Hilbert space V, whose norm is denoted here by $\|\cdot\|_V$. In particular, $L^2_{[0,T]}(V)$ is the space of classes of functions $f : (0,T) \to V$ that are Böchner–measurable and such that $\|f\|_{L^2_{[0,T]}(V)} < \infty$, with

$$\|f\|^2_{L^2_{[0,T]}(V)} := \int_0^T \|f(t)\|^2_V \, \mathrm{d}t.$$

We use the notation $C^0_{[0,T]}(V)$ for the Banach space consisting of all continuous functions $f : [0,T] \to V$. More generally, for any $k \in \mathbb{N}$, $C^k_{[0,T]}(V)$ denotes the subspace of $C^0_{[0,T]}(V)$ of all functions f with (strong) derivatives $\frac{\mathrm{d}^j f}{\mathrm{d}t^j}$ in $C^0_{[0,T]}(V)$ for all $1 \le j \le k$. In what follows, we will use indistinctly the notations $\dot f := \frac{\mathrm{d}f}{\mathrm{d}t}$, $\ddot f := \frac{\mathrm{d}^2 f}{\mathrm{d}t^2}$, and $\dddot f := \frac{\mathrm{d}^3 f}{\mathrm{d}t^3}$ to express the first, second, and third derivatives with respect to t. Furthermore, we consider the Sobolev space

$$H^1_{[0,T]}(V) := \left\{ f : \ \exists g \in L^2_{[0,T]}(V) \text{ and } \exists f_0 \in V \text{ such that } f(t) = f_0 + \int_0^t g(s)\,\mathrm{d}s \quad \forall t \in [0,T] \right\}.$$

2. A mixed variational formulation of the Zener model

Our objective is to study the dynamics of a viscoelastic body with mass density ρ governed by the equation of motion:

$$\rho \ddot{\boldsymbol{d}} - \mathbf{div}\,\boldsymbol{\sigma} = \boldsymbol{f} \quad \text{in } \Omega \times (0,T],$$

where Ω is a polygonal or polyhedral Lipschitz domain in $\mathbb{R}^d$ ($d = 2, 3$), and $\boldsymbol{f} : \Omega \times [0,T] \to \mathbb{R}^d$ represents the body force acting over the time interval $[0,T]$. The vector field $\boldsymbol{d} : \Omega \times [0,T] \to \mathbb{R}^d$ is the displacement and $\boldsymbol{\sigma} : \Omega \times [0,T] \to \mathbb{S}$ is the stress tensor. The linearized strain tensor $\boldsymbol{\varepsilon}(\boldsymbol{d})$ is related to the stress through Zener's constitutive law for viscoelasticity (see [2]):

$$\boldsymbol{\sigma} + \omega \dot{\boldsymbol{\sigma}} = C\boldsymbol{\varepsilon}(\boldsymbol{d}) + \omega D \boldsymbol{\varepsilon}(\dot{\boldsymbol{d}}) \quad \text{in } \Omega \times (0,T], \tag{2.1}$$

where C and D are two symmetric and positive definite tensors of order 4. To guarantee that the system is dissipative we assume that $D - C$ is also positive definite, see [5]. Additionally, we assume that the coefficients of the tensors C and D, the mass density ρ, and the relaxation time ω are piecewise constant functions. More specifically, we assume that there exists a disjoint partition of $\bar\Omega$ into polygonal/polyhedral subdomains $\{\bar\Omega_j, \ j = 1, \dots, J\}$ such that $C_j := C|_{\Omega_j}$, $D_j := D|_{\Omega_j}$, $\rho_j := \rho|_{\Omega_j} > 0$ and $\omega_j := \omega|_{\Omega_j} \ge 0$ for $j = 1, \dots, J$. According to our assumption on the tensors C and D, there exist constants $d^+ > c^+ > 0$ and $d^- > c^- > 0$ such that

$$c^- \boldsymbol{\zeta} : \boldsymbol{\zeta} \le C_j \boldsymbol{\zeta} : \boldsymbol{\zeta} \le c^+ \boldsymbol{\zeta} : \boldsymbol{\zeta} \quad \text{and} \quad d^- \boldsymbol{\zeta} : \boldsymbol{\zeta} \le D_j \boldsymbol{\zeta} : \boldsymbol{\zeta} \le d^+ \boldsymbol{\zeta} : \boldsymbol{\zeta} \quad \forall \boldsymbol{\zeta} \in \mathbb{S}, \quad \forall j = 1, \dots, J. \tag{2.2}$$

We point out that, in the regions Ω_j where the piecewise constant function ω is zero, the constitutive law (2.1) becomes the familiar Hooke's Law. Hence, it is natural to introduce the set of indices $\mathcal{I}_E := \{j \in \{1, \dots, J\} : \ \omega_j = 0\}$ and $\mathcal{I}_V := \{j \in \{1, \dots, J\} : \ \omega_j > 0\}$ and to split Ω into a part $\Omega_E := \cup_{j \in \mathcal{I}_E} \Omega_j$ displaying a purely elastic behavior and a part $\Omega_V := \cup_{j \in \mathcal{I}_V} \Omega_j$ exhibiting viscoelastic properties. The reciprocal $\tilde\omega^{-1}$ of the relaxation time ω in Ω_V is extended by zero to Ω_E, i.e.,

$$\tilde\omega^{-1}|_{\Omega_j} := \begin{cases} \omega_j^{-1} & \text{if } j \in \mathcal{I}_V, \\ 0 & \text{if } j \in \mathcal{I}_E, \end{cases} \quad j = 1, \dots, J.$$

We assume that the viscoelastic body is clamped ($\boldsymbol{d} = \boldsymbol{0}$) at $\Gamma_D \times (0,T]$, where the boundary subset $\Gamma_D \subset \Gamma := \partial\Omega$ is of positive surface measure. Additionally, we assume that it is free of stress ($\boldsymbol{\sigma}\boldsymbol{n} = \boldsymbol{0}$) on $\Gamma_N \times (0,T]$, where $\Gamma_N := \Gamma \setminus \Gamma_D$ and $\boldsymbol{n}$ is the exterior unit normal vector on Γ. Finally, we impose the initial conditions

$$\boldsymbol{d}(0) = \boldsymbol{d}^0 \quad \text{in } \Omega, \quad \dot{\boldsymbol{d}}(0) = \boldsymbol{d}^1 \quad \text{in } \Omega, \quad \text{and} \quad \boldsymbol{\sigma}(0) = \boldsymbol{\sigma}^0 \quad \text{in } \Omega_V. \tag{2.3}$$

Our aim is to impose the stress tensor $\boldsymbol{\sigma}$ as a primary unknown. To this end, we follow [5] and decompose this variable into a purely elastic component $\boldsymbol{\sigma}_E := C\boldsymbol{\varepsilon}(\boldsymbol{d})$ and a viscoelastic component $\omega\boldsymbol{\sigma}_V := \boldsymbol{\sigma} - \boldsymbol{\sigma}_E$. Hence, if we adopt the notations $\mathcal{A} := C^{-1}$ and $\mathcal{G} := (D - C)^{-1}$, our model problem can be written as follows in terms of $\boldsymbol{d}$, $\boldsymbol{\sigma}_E$, $\boldsymbol{\sigma}_V$ and $\boldsymbol{\sigma} = \boldsymbol{\sigma}_E + \omega\boldsymbol{\sigma}_V$ (see [9] for more details):

$$\begin{aligned} \rho \ddot{\boldsymbol{d}} - \mathbf{div}\,\boldsymbol{\sigma} &= \boldsymbol{f} \quad \text{in } \Omega \times (0,T], \\ \mathcal{A}\ddot{\boldsymbol{\sigma}}_E &= \boldsymbol{\varepsilon}(\ddot{\boldsymbol{d}}) \quad \text{in } \Omega \times (0,T], \\ \omega^2 \mathcal{G}\ddot{\boldsymbol{\sigma}}_V + \omega\mathcal{G}\dot{\boldsymbol{\sigma}}_V &= \omega\boldsymbol{\varepsilon}(\ddot{\boldsymbol{d}}) \quad \text{in } \Omega \times (0,T], \\ \boldsymbol{d} &= \boldsymbol{0} \quad \text{on } \Gamma_D \times (0,T], \\ \boldsymbol{\sigma}\boldsymbol{n} &= \boldsymbol{0} \quad \text{on } \Gamma_N \times (0,T]. \end{aligned} \tag{2.4}$$

We consider the space $L^2_V(\Omega, \mathbb{S}) := \{\boldsymbol{\tau}_V \in L^2(\Omega, \mathbb{S}); \ \boldsymbol{\tau}_V|_{\Omega_E} = \boldsymbol{0}\}$ and introduce $\mathcal{H} := L^2(\Omega, \mathbb{S}) \times L^2_V(\Omega, \mathbb{S})$ endowed with the inner product

$$(\underline{\boldsymbol{\sigma}}, \underline{\boldsymbol{\tau}})_{\mathcal{H}} := (\mathcal{A}\boldsymbol{\sigma}_E, \boldsymbol{\tau}_E)_\Omega + (\mathcal{G}\omega\boldsymbol{\sigma}_V, \omega\boldsymbol{\tau}_V)_\Omega \quad \underline{\boldsymbol{\sigma}} := (\boldsymbol{\sigma}_E, \boldsymbol{\sigma}_V), \quad \underline{\boldsymbol{\tau}} := (\boldsymbol{\tau}_E, \boldsymbol{\tau}_V) \in \mathcal{H},$$

whose associated norm is $\|\underline{\boldsymbol{\tau}}\|^2_{\mathcal{H}} := (\mathcal{A}\boldsymbol{\tau}_E, \boldsymbol{\tau}_E)_\Omega + (\mathcal{G}\omega\boldsymbol{\tau}_V, \omega\boldsymbol{\tau}_V)_\Omega$. By virtue of (2.2), we have that

$$c_* \sum_{j=1}^J (\|\boldsymbol{\tau}_E\|^2_{0,\Omega_j} + \omega_j^2 \|\boldsymbol{\tau}_V\|^2_{0,\Omega_j}) \le \|\underline{\boldsymbol{\tau}}\|^2_{\mathcal{H}} \le c^* \sum_{j=1}^J (\|\boldsymbol{\tau}_E\|^2_{0,\Omega_j} + \omega_j^2 \|\boldsymbol{\tau}_V\|^2_{0,\Omega_j}) \quad \forall \underline{\boldsymbol{\tau}} \in \mathcal{H}, \tag{2.5}$$

with $c^* = \max\{\frac{1}{c^-}, \frac{1}{d^- - c^-}\}$ and $c_* = \min\{\frac{1}{c^+}, \frac{1}{d^+ - c^+}\}$. We denote by

$$H_N(\mathbf{div}, \Omega, \mathbb{S}) := \{\boldsymbol{\tau} \in H(\mathbf{div}, \Omega, \mathbb{S}); \quad \langle \boldsymbol{\tau}\boldsymbol{n}, \boldsymbol{u}\rangle_\Gamma = 0 \quad \forall \boldsymbol{u} \in H^1_D(\Omega, \mathbb{R}^d)\},$$

the closed subspace of $H(\mathbf{div}, \Omega, \mathbb{S})$ that incorporates the stress free boundary condition on Γ_N. Here, $H^1_D(\Omega, \mathbb{R}^d) := \{\boldsymbol{v} \in H^1(\Omega, \mathbb{R}^d);\ \boldsymbol{v}|_{\Gamma_D} = \mathbf{0}\}$ and $\langle\cdot,\cdot\rangle_\Gamma$ stands for the duality pairing between $H^{1/2}(\Gamma, \mathbb{R}^d)$ and $H^{-1/2}(\Gamma, \mathbb{R}^d)$. The natural energy space for the pair of tensors $\underline{\boldsymbol{\sigma}}(t) := (\boldsymbol{\sigma}_E, \boldsymbol{\sigma}_V) \in \mathcal{H}$ representing the elastic and viscoelastic components of the stress $\boldsymbol{\sigma} := \boldsymbol{\sigma}_E + \omega\boldsymbol{\sigma}_V$ is given by

$$\mathcal{X}^+ := \{\underline{\boldsymbol{\tau}} := (\boldsymbol{\tau}_E, \boldsymbol{\tau}_V) \in \mathcal{H};\ \boldsymbol{\tau} := \boldsymbol{\tau}_E + \omega\boldsymbol{\tau}_V \in H_N(\mathbf{div}, \Omega, \mathbb{S})\}.$$

It is endowed with the Hilbertian norm $\|\underline{\boldsymbol{\tau}}\|^2_{\mathcal{X}^+} := \|\underline{\boldsymbol{\tau}}\|^2_{\mathcal{H}} + \|\mathbf{div}\,\boldsymbol{\tau}\|^2_{0,\Omega}$.

We know from [9, Lemma 3.1] that the embedding $\mathcal{X}^+ \hookrightarrow \mathcal{H}$ is dense. We can then consider the dual $(\mathcal{X}^+)'$ of $\mathcal{X}^+$ pivotal to $\mathcal{H}$, and denote by $\langle\cdot,\cdot\rangle_{(\mathcal{X}^+)'\times\mathcal{X}^+}$ the corresponding the duality pairing. It is well-known that if $\boldsymbol{\sigma} \in L^2_{[0,T]}(\mathcal{X}^+)$ is such that $\dot{\boldsymbol{\sigma}} \in L^2_{[0,T]}((\mathcal{X}^+)')$, then the identity

$$\frac{\mathrm{d}}{\mathrm{d}t}(\underline{\boldsymbol{\sigma}}(t), \underline{\boldsymbol{\tau}})_{\mathcal{H}} = \langle \underline{\dot{\boldsymbol{\sigma}}}(t), \underline{\boldsymbol{\tau}}\rangle_{(\mathcal{X}^+)'\times\mathcal{X}^+} \quad \forall \underline{\boldsymbol{\tau}} \in \mathcal{X}^+$$

holds true in the sense of distributions on $(0, T)$. With this property at hand, we can now introduce the Hilbert space

$$W(\mathcal{X}^+, (\mathcal{X}^+)') := \{\underline{\boldsymbol{\tau}} \in H^1_{[0,T]}(\mathcal{X}^+) :\ \ddot{\underline{\boldsymbol{\tau}}} \in L^2_{[0,T]}((\mathcal{X}^+)')\},$$

and consider the following pure-stress variational formulation of problem (2.4) (see [9] for more details): find $\underline{\boldsymbol{\sigma}} = (\boldsymbol{\sigma}_E, \boldsymbol{\sigma}_V) \in W(\mathcal{X}^+, (\mathcal{X}^+)')$ such that

$$\frac{\mathrm{d}}{\mathrm{d}t}(\underline{\dot{\boldsymbol{\sigma}}}, \underline{\boldsymbol{\tau}})_{\mathcal{H}} + (\mathcal{G}\dot{\boldsymbol{\sigma}}_V, \omega\boldsymbol{\tau}_V)_\Omega + (\rho^{-1}\mathbf{div}\,\boldsymbol{\sigma}, \mathbf{div}\,\boldsymbol{\tau})_\Omega = -(\rho^{-1}\boldsymbol{f}, \mathbf{div}\,\boldsymbol{\tau})_\Omega \quad \forall \underline{\boldsymbol{\tau}} = (\boldsymbol{\tau}_E, \boldsymbol{\tau}_V) \in \mathcal{X}^+, \tag{2.6}$$

with the initial conditions $\underline{\boldsymbol{\sigma}}(0) = \underline{\boldsymbol{\sigma}}^0$ and $\underline{\dot{\boldsymbol{\sigma}}}(0) = \underline{\boldsymbol{\sigma}}^1$, where

$$\begin{aligned} &\underline{\boldsymbol{\sigma}}^0 = (\boldsymbol{\sigma}^0_E, \boldsymbol{\sigma}^0_V) \quad \text{with} \quad \boldsymbol{\sigma}^0_E := C\boldsymbol{\varepsilon}(\boldsymbol{d}^0), \quad \boldsymbol{\sigma}^0_V := \tilde{\omega}^{-1}\big(\boldsymbol{\sigma}^0 - \boldsymbol{\sigma}^0_E\big) \quad \text{and} \\ &\underline{\boldsymbol{\sigma}}^1 = (\boldsymbol{\sigma}^1_E, \boldsymbol{\sigma}^1_V) \quad \text{with} \quad \boldsymbol{\sigma}^1_E := C\boldsymbol{\varepsilon}(\boldsymbol{d}^1), \quad \boldsymbol{\sigma}^1_V := \tilde{\omega}^{-1}\big((\mathcal{D} - C)\boldsymbol{\varepsilon}(\boldsymbol{d}^1) - \boldsymbol{\sigma}^0_V\big). \end{aligned} \tag{2.7}$$

Theorem 2.1. *Assume that the problem data satisfy $\boldsymbol{d}^0, \boldsymbol{d}^1 \in H^1_D(\Omega, \mathbb{R}^d)$, $\boldsymbol{\sigma}^0 \in H_N(\mathbf{div}, \Omega, \mathbb{S})$ and $\boldsymbol{f} \in H^1_{[0,T]}(L^2(\Omega, \mathbb{R}^d))$. Then, problem (2.6)–(2.7) admits a unique solution. Moreover, there exists a constant $C > 0$ such that*

$$\max_{t\in[0,T]} \|\underline{\boldsymbol{\sigma}}(t)\|_{\mathcal{X}^+} + \max_{t\in[0,T]} \|\underline{\dot{\boldsymbol{\sigma}}}(t)\|_{\mathcal{H}} \le C\Big(\|\boldsymbol{f}\|_{H^1_{[0,T]}(L^2(\Omega,\mathbb{R}^d))} + \|\underline{\boldsymbol{\sigma}}^0\|_{\mathcal{X}^+} + \|\underline{\boldsymbol{\sigma}}^1\|_{\mathcal{H}}\Big). \tag{2.8}$$

Proof. The result is proved in [9, Theorem 4.1] by resorting to energy estimates and a classical Galerkin procedure. See also [8,29] for similar strategies applied to mixed formulations in elastodynamics and viscoelasticity. □

We point out that an HDG method based on the primal mixed formulation (2.6) results in a numerical approach that is similar to the one presented in [30]. This method approximates the dual flux variable $\boldsymbol{\sigma}\boldsymbol{n}$ by a piecewise polynomials on the interelement boundaries of the mesh that are defined up to sign changes on each facet, which gives rise to some computational disadvantages. Actually, we use here the variational formulation (2.6) solely as an intermediate step for deducing and analyzing the velocity/stress formulation [5–7] of problem (2.4). This variational formulation consists in finding a vector field $\boldsymbol{u} \in C^1_{[0,T]}(L^2(\Omega, \mathbb{R}^d)) \cap C^0_{[0,T]}(H^1_D(\Omega, \mathbb{R}^d))$ and a couple of tensors $\underline{\boldsymbol{\sigma}} \in H^1_{[0,T]}(\mathcal{X}^+) \cap C^1_{[0,T]}(\mathcal{H})$ satisfying the first-order system in time

$$\begin{aligned} &(\rho\dot{\boldsymbol{u}}, \boldsymbol{v})_\Omega - (\mathbf{div}\,\boldsymbol{\sigma}, \boldsymbol{v})_\Omega = (\boldsymbol{f}, \boldsymbol{v})_\Omega \quad \forall \boldsymbol{v} \in L^2(\Omega, \mathbb{R}^d), \\ &(\underline{\dot{\boldsymbol{\sigma}}}, \underline{\boldsymbol{\tau}})_{\mathcal{H}} + (\mathcal{G}\boldsymbol{\sigma}_V, \omega\boldsymbol{\tau}_V)_\Omega + (\boldsymbol{u}, \mathbf{div}\,\boldsymbol{\tau})_\Omega = 0 \quad \forall \underline{\boldsymbol{\tau}} = (\boldsymbol{\tau}_E, \boldsymbol{\tau}_V) \in \mathcal{X}^+, \end{aligned} \tag{2.9}$$

and subject to the initial conditions

$$\boldsymbol{u}(0) = \boldsymbol{d}^1 \quad \text{and} \quad \underline{\boldsymbol{\sigma}}(0) = \underline{\boldsymbol{\sigma}}^0. \tag{2.10}$$

Proposition 2.1. *Under the conditions of Theorem 2.1, $\underline{\boldsymbol{\sigma}} = (\boldsymbol{\sigma}_E, \boldsymbol{\sigma}_V) \in W(\mathcal{X}^+, (\mathcal{X}^+)')$ is a solution of problem (2.6)–(2.7) if and only if the pair $(\underline{\boldsymbol{\sigma}}, \boldsymbol{u})$ is a solution of problem (2.9)–(2.10), where the velocity field is given by*

$$\boldsymbol{u}(t) := \int_0^t \rho^{-1}(\boldsymbol{f} + \mathbf{div}\,\boldsymbol{\sigma})(s)\,ds + \boldsymbol{d}^1. \tag{2.11}$$

Proof. Let $\underline{\boldsymbol{\sigma}} \in W(\mathcal{X}^+, (\mathcal{X}^+)')$ be the solution of (2.6). We observe that the embeddings

$$H^1_{[0,T]}(\mathcal{X}^+) \hookrightarrow C^0_{[0,T]}(\mathcal{X}^+) \quad \text{and} \quad W(\mathcal{X}^+, (\mathcal{X}^+)') \hookrightarrow C^0_{[0,T]}(\mathcal{H})$$

(see [31, Chapter XVIII, Section 1, Theorem 1]) ensure that $\underline{\boldsymbol{\sigma}}$ belongs to $C^0_{[0,T]}(\mathcal{X}^+) \cap C^1_{[0,T]}(\mathcal{H})$, while the reconstructed velocity field (2.11) belongs to $C^1(L^2(\Omega, \mathbb{R}^d))$. Integrating Eq. (2.6) over the time interval $[0, t]$ with $t \le T$ and considering the initial conditions (2.7), we easily deduce that

$$(\underline{\dot{\boldsymbol{\sigma}}}, \underline{\boldsymbol{\tau}})_{\mathcal{H}} + (\mathcal{G}\boldsymbol{\sigma}_V, \omega\boldsymbol{\tau}_V)_\Omega + (\boldsymbol{u}, \mathbf{div}\,\boldsymbol{\tau})_\Omega = 0 \quad \forall \underline{\boldsymbol{\tau}} = (\boldsymbol{\tau}_E, \boldsymbol{\tau}_V) \in \mathcal{X}^+. \tag{2.12}$$

Testing Eq. (2.12) with $\underline{\boldsymbol{\tau}} = (\boldsymbol{\eta}, \mathbf{0})$, where the components of the tensor $\boldsymbol{\eta} : \Omega \to \mathbb{S}$ are indefinitely differentiable and have compact support contained in Ω, we obtain $\boldsymbol{\epsilon}(\boldsymbol{u}) = \mathcal{A}\dot{\boldsymbol{\sigma}}_E \in C^0_{[0,T]}(L^2(\Omega, \mathbb{S}))$. Using Korn's inequality, we further conclude that $\boldsymbol{u} \in C^0_{[0,T]}(H^1(\Omega, \mathbb{R}^d))$. Next, testing Eq. (2.12) with $\underline{\boldsymbol{\tau}} = (\boldsymbol{\eta}, \mathbf{0})$, where $\boldsymbol{\eta} \in H_N(\mathbf{div}, \Omega, \mathbb{S})$ and applying Green's formula (1.2) prove that $\boldsymbol{u} \in C^0_{[0,T]}(H^1_D(\Omega, \mathbb{R}^d))$. In summary, $\underline{\boldsymbol{\sigma}} \in H^1_{[0,T]}(\mathcal{X}^+) \cap C^1_{[0,T]}(\mathcal{H})$ and $\boldsymbol{u} \in C^1_{[0,T]}(L^2(\Omega, \mathbb{R}^d)) \cap C^0_{[0,T]}(H^1_D(\Omega, \mathbb{R}^d))$ are solutions to (2.9) since they satisfy the second equation of the system by virtue of (2.12) and the first equation of the system is deduced by taking the time derivative of (2.11), multiplying by ρ and testing the resulting identity with $\boldsymbol{v} \in L^2(\Omega, \mathbb{R}^d)$. Furthermore, the initial conditions (2.10) are trivially satisfied.

Reciprocally, let $\underline{\boldsymbol{\sigma}} \in H^1_{[0,T]}(\mathcal{X}^+) \cap C^1_{[0,T]}(\mathcal{H})$ and $\boldsymbol{u} \in C^1_{[0,T]}(L^2(\Omega, \mathbb{R}^d)) \cap C^0_{[0,T]}(H^1_D(\Omega, \mathbb{R}^d))$ be the solution of (2.9)–(2.10). We deduce from the first equation of (2.9) that

$$\dot{\boldsymbol{u}} = \rho^{-1}\big(\boldsymbol{f} + \mathbf{div}\,\boldsymbol{\sigma}\big) \tag{2.13}$$

and computing the time de derivative of the second one in the sense of distributions yields

$$\frac{\mathrm{d}}{\mathrm{d}t}(\underline{\boldsymbol{\sigma}}, \underline{\boldsymbol{\tau}})_{\mathcal{H}} + (\mathcal{G}\dot{\boldsymbol{\sigma}}_V, \omega\boldsymbol{\tau}_V)_{\Omega} + (\dot{\boldsymbol{u}}, \mathbf{div}\,\boldsymbol{\tau})_{\Omega} = 0. \tag{2.14}$$

We deduce from Eq. (2.14) that $\underline{\boldsymbol{\sigma}}$ belongs to the space $W(\mathcal{X}^+, (\mathcal{X}^+)')$. Moreover, combining Eqs. (2.13) and (2.14), we can eliminate the velocity field and prove that $\underline{\boldsymbol{\sigma}}$ solves problem (2.6). Furthermore, the initial conditions (2.7) can be easily inferred from the second equation of (2.9). □

Remark 2.1. As a consequence of Theorem 2.1 and Proposition 2.1, problem (2.9)–(2.10) is also well-posed. We point out that the stress/velocity formulation of problem (2.4) can also be analyzed using the theory of continuous semigroups of bounded linear operators, as demonstrated in [5,7].

3. Finite element spaces and auxiliary results

For the sake of simplicity, we assume from now on that the structure is clamped along its entire boundary, that is, $\Gamma_D = \Gamma$. As a result, we have

$$\mathcal{X}^+ = \{\underline{\boldsymbol{\tau}} = (\boldsymbol{\tau}_E, \boldsymbol{\tau}_V) \in \mathcal{H} \mid \boldsymbol{\tau} := \boldsymbol{\tau}_E + \omega\boldsymbol{\tau}_V \in H(\mathbf{div}, \Omega, \mathbb{S})\}$$

and $\boldsymbol{u} \in C^0_{[0,T]}(H^1_0(\Omega, \mathbb{R}^d))$, with the usual notation $H^1_0(\Omega, \mathbb{R}^d) := \{\boldsymbol{v} \in H^1(\Omega, \mathbb{R}^d),\ \boldsymbol{v}|_\Gamma = \mathbf{0}\}$.

Let $\mathcal{T}_h$ be a shape regular triangulation of the domain $\bar{\Omega}$ into tetrahedra and/or parallelepipeds if $d = 3$ and into triangles and/or quadrilaterals if $d = 2$. We allow $\mathcal{T}_h$ to have hanging nodes and assume that it is aligned with the interfaces between different materials. Specifically, for any $j = 1, \ldots, J$, $\bar{\Omega}_j$ coincides with the union of the elements of the set $\mathcal{T}_h(\Omega_j) := \{K \in \mathcal{T}_h;\ K \subset \bar{\Omega}_j\}$. As a consequence, $\mathcal{A}$ and $\mathcal{G}$ are constant tensors and ρ and ω are constant functions within each element of $\mathcal{T}_h$. We denote by h_K the diameter of K and let the parameter $h := \max_{K\in\mathcal{T}_h}\{h_K\}$ represent the size of the mesh $\mathcal{T}_h$.

We define a closed subset $F \subset \overline{\Omega}$ to be an interior edge/face if it has a positive $(d-1)$-dimensional measure and can be expressed as the intersection of the closures of two distinct elements K and K', i.e., $F = \bar{K} \cap \bar{K}'$. On the other hand, a closed subset $F \subset \overline{\Omega}$ is a boundary edge/face if there exists $K \in \mathcal{T}_h$ such that F is an edge/face of K and $F = \bar{K} \cap \partial\Omega$. We consider the set $\mathcal{F}_h^0$ of interior edges/faces and the set $\mathcal{F}_h^\partial$ of boundary edges/faces and let $\mathcal{F}_h = \mathcal{F}_h^0 \cup \mathcal{F}_h^\partial$. We denote by h_F the diameter an edge/face $F \in \mathcal{F}_h$ and make the assumption that $\mathcal{T}_h$ is locally quasi-uniform with constant $\gamma > 0$. This means that, for all h and all $K \in \mathcal{T}_h$, we have that

$$h_F \le h_K \le \gamma h_F \quad \forall F \in \mathcal{F}(K), \tag{3.1}$$

where $\mathcal{F}(K)$ represents the set of edges/faces composing the element $K \in \mathcal{T}_h$. This condition implies that neighboring elements have similar sizes.

Throughout the rest of this paper, we shall use the letters C and c to denote generic positive constants independent of the mesh size h, the polynomial degree k and the relaxation time ω. These constants may stand for different values at its different occurrences. Moreover, given any positive expressions X and Y depending on h, k, and ω, the notation $X \lesssim Y$ means that $X \le CY$.

For all $s \ge 0$, the broken Sobolev space with respect to the partition $\mathcal{T}_h$ of $\bar{\Omega}$ is defined as

$$H^s(\mathcal{T}_h, E) := \{\boldsymbol{v} \in L^2(\Omega, E) : \quad \boldsymbol{v}|_K \in H^s(K, E) \quad \forall K \in \mathcal{T}_h\}, \quad \text{for } E \in \{\mathbb{R}, \mathbb{R}^d, \mathbb{S}\}.$$

Following the convention mentioned earlier, we write $H^0(\mathcal{T}_h, E) = L^2(\mathcal{T}_h, E)$ and $H^s(\mathcal{T}_h, \mathbb{R}) = H^s(\mathcal{T}_h)$. We introduce the inner product

$$(\psi, \varphi)_{\mathcal{T}_h} := \sum_{K\in\mathcal{T}_h} (\psi, \varphi)_K \quad \forall \psi, \varphi \in L^2(\mathcal{T}_h, E), \quad E \in \{\mathbb{R}, \mathbb{R}^d, \mathbb{S}\}$$

and write $\|\psi\|^2_{0,\mathcal{T}_h} := (\psi, \psi)_{\mathcal{T}_h}$. Accordingly, we let $\partial\mathcal{T}_h := \{\partial K;\ K \in \mathcal{T}_h\}$ be the set of all element boundaries and define $L^2(\partial\mathcal{T}_h, \mathbb{R}^d)$ as the space of vector-valued functions which are square-integrable on each $\partial K \in \partial\mathcal{T}_h$. We define

$$\langle \boldsymbol{u}, \boldsymbol{v}\rangle_{\partial\mathcal{T}_h} := \sum_{K\in\mathcal{T}_h} \langle \boldsymbol{u}, \boldsymbol{v}\rangle_{\partial K}, \quad \text{and} \quad \|\boldsymbol{v}\|^2_{0,\partial\mathcal{T}_h} := \langle \boldsymbol{v}, \boldsymbol{v}\rangle_{\partial\mathcal{T}_h} \quad \forall \boldsymbol{u}, \boldsymbol{v} \in L^2(\partial\mathcal{T}_h, \mathbb{R}^d),$$

where $\langle \boldsymbol{u}, \boldsymbol{v}\rangle_{\partial K} := \sum_{F\in\mathcal{F}(K)} \int_F \boldsymbol{u}\cdot\boldsymbol{v}$. Besides, we equip the space $L^2(\mathcal{F}_h,\mathbb{R}^d) := \prod_{F\in\mathcal{F}_h} L^2(F,\mathbb{R}^d)$ with the inner product

$$(\boldsymbol{u},\boldsymbol{v})_{\mathcal{F}_h} := \sum_{F\in\mathcal{F}_h}\int_F \boldsymbol{u}\cdot\boldsymbol{v} \quad \forall \boldsymbol{u},\boldsymbol{v}\in L^2(\mathcal{F}_h,\mathbb{R}^d),$$

and denote the corresponding norm $\|\boldsymbol{v}\|^2_{0,\mathcal{F}_h} := (\boldsymbol{v},\boldsymbol{v})_{\mathcal{F}_h}$.

Hereafter, $\mathcal{P}_m(D)$ is the space of polynomials of degree at most $m\geq 0$ on D if D is a triangle/tetrahedron, and the space of polynomials of degree at most m in each variable in D if D is a quadrilateral/parallelepiped. The space of E-valued functions with components in $\mathcal{P}_m(D)$ is denoted $\mathcal{P}_m(D,E)$ where E is either $\mathbb{R}^d$, or $\mathbb{S}$. We introduce the space of piecewise-polynomial functions

$$\mathcal{P}_m(\mathcal{T}_h) := \{v\in L^2(\mathcal{T}_h):\ v|_K\in\mathcal{P}_m(K),\ \forall K\in\mathcal{T}_h\}$$

with respect to the partition $\mathcal{T}_h$ and the space of piecewise-polynomial functions

$$\mathcal{P}_m(\mathcal{F}_h) := \{\hat{\boldsymbol{v}}\in L^2(\mathcal{F}_h):\ \hat{\boldsymbol{v}}|_F\in\mathcal{P}_m(F),\ \forall F\in\mathcal{F}_h\}$$

with respect to the partition $\mathcal{F}_h$. The subspace of $L^2(\mathcal{T}_h,E)$ with components in $\mathcal{P}_m(\mathcal{T}_h)$ is denoted $\mathcal{P}_m(\mathcal{T}_h,E)$ for $E\in\{\mathbb{R}^d,\mathbb{S}\}$. Likewise, $\mathcal{P}_m(\mathcal{F}_h,\mathbb{R}^d)$ stands for the subspace of $L^2(\mathcal{F}_h,\mathbb{R}^d)$ with components in $\mathcal{P}_m(\mathcal{F}_h)$. We finally consider

$$\mathcal{P}_m(\partial\mathcal{T}_h,\mathbb{R}^d) := \{\boldsymbol{v}\in L^2(\partial\mathcal{T}_h,\mathbb{R}^d);\ \boldsymbol{v}|_{\partial K}\in\mathcal{P}_m(\partial K,\mathbb{R}^d),\ \forall K\in\mathcal{T}_h\},$$

where $\mathcal{P}_m(\partial K,\mathbb{R}^d) := \prod_{F\in\mathcal{F}(K)}\mathcal{P}_m(F,\mathbb{R}^d)$. It is worth noting that, by definition, the functions in $L^2(\partial\mathcal{T}_h,\mathbb{R}^d)$ and $\mathcal{P}_m(\partial\mathcal{T}_h,\mathbb{R}^d)$ are multi-valued on every interior face F, whereas the functions in $L^2(\mathcal{F}_h,\mathbb{R}^d)$ and $\mathcal{P}_m(\mathcal{F}_h,\mathbb{R}^d)$ are single-valued on each face F.

In the rest of this section, we recall some well-known local hp estimates and use them to obtain global hp estimates that will be used in the subsequent analysis. we first present the following inverse inequalities, which can be found in [32, Theorem 1] and [33, Theorem 4.76].

Lemma 3.1. *There exists a constant $C>0$ independent of h and m such that*

$$\frac{m+1}{h_K^{1/2}}\|v\|_{0,\partial K}+\|\nabla v\|_{0,K}\leq C\frac{(m+1)^2}{h_K}\|v\|_{0,K}\quad \forall v\in\mathcal{P}_m(K),\quad \forall K\in\mathcal{T}_h,\ m\geq 0. \tag{3.2}$$

For any integer $m\geq 0$ and $K\in\mathcal{T}_h$, we denote by Π_K^m the $L^2(K)$-orthogonal projection onto $\mathcal{P}_m(K)$. The global projection $\Pi_{\mathcal{T}}^m$ in $L^2(\mathcal{T}_h)$ onto $\mathcal{P}_m(\mathcal{T}_h)$ is then given by $(\Pi_{\mathcal{T}}^m v)|_K=\Pi_K^m(v|_K)$ for all $K\in\mathcal{T}_h$. Similarly, the global projection $\Pi_{\mathcal{F}}^m$ in $L^2(\mathcal{F}_h)$ onto $\mathcal{P}_m(\mathcal{F}_h)$ is given, separately for all $F\in\mathcal{F}_h$, by $(\Pi_{\mathcal{F}}^m\hat{v})|_F=\Pi_F^m(\hat{v}|_F)$, where Π_F^m is the $L^2(F)$-orthogonal projection onto $\mathcal{P}_m(F)$. In the following lemma, we recall local approximation properties for these projectors.

Proposition 3.1. *Let $K\in\mathcal{T}_h$ and assume that $u\in H^{1+s}(K)$, with $s\geq 0$. There exists a constant $C>0$ independent of h and m such that*

$$\|u-\Pi_K^m u\|_{0,K}+\frac{h_K}{(m+1)^{3/2}}\|\nabla(u-\Pi_K^m u)\|_{0,K}\leq C\frac{h_K^{\min\{s,m\}+1}}{(m+1)^{s+1}}\|u\|_{s+1,K}\quad m\geq 0, \tag{3.3}$$

and

$$\|u-\Pi_K^m u\|_{0,\partial K}+\|u-\Pi_F^m u\|_{0,F}\leq C\frac{h_K^{\min\{s,m\}+1/2}}{(m+1)^{s+1/2}}\|u\|_{s+1,K}\quad \forall F\in\mathcal{F}(K),\quad m\geq 0. \tag{3.4}$$

Proof. The proof relies on the hp-approximation results provided for two-dimensional elements in [34, Lemma 4.5], which are also applicable to three-dimensional elements. Specifically, if $u\in H^{1+s}(K)$, with $s\geq 0$, the result guarantees the existence of a sequence of polynomials $\{u_m\in\mathcal{P}_m(K);\ m=0,1,\ldots\}$ satisfying

$$\|u-u_m\|_{0,K}+\frac{h_K}{m+1}\|\nabla(u-u_m)\|_{0,K}\leq c\frac{h_K^{\min\{s,m\}+1}}{(m+1)^{s+1}}\|u\|_{s+1,K}, \tag{3.5}$$

with $c>0$ independent of h and m. Due to the optimality of the L^2-projection, it follows immediately that

$$\|u-\Pi_K^m u\|_{0,K}\leq\|u-u_m\|_{0,K}\leq c\frac{h_K^{\min\{s,m\}+1}}{(m+1)^{s+1}}\|u\|_{s+1,K}.$$

Moreover, it is shown in [35, Corollary 1.3] that

$$\|\nabla\Pi_K^m w\|_{0,K}\lesssim m^{1/2}\|\nabla w\|_{0,K}\quad \forall w\in H^1(K).$$

Taking $w=u-u_m$ in the last inequality and using (3.5) yield

$$\|\nabla(u_m-\Pi_K^m u)\|_{0,K}\lesssim m^{1/2}\|\nabla(u-u_m)\|_{0,K}\lesssim\frac{h_K^{\min\{s,m\}}}{(m+1)^{s-1/2}}\|u\|_{s+1,K}.$$

Using the last bound in the triangle inequality

$$\|\nabla(u-\Pi_K^m u)\|_{0,K}\leq\|\nabla(u-u_m)\|_{0,K}+\|\nabla(u_m-\Pi_K^m u)\|_{0,K}$$

we obtain the estimate corresponding to the H^1–seminorm in (3.3). On the other hand, we deduce from [35, Corollary 1.2] and a standard scaling argument that

$$\|w - \Pi_K^m w\|_{0,\partial K} \lesssim \sqrt{\tfrac{h_K}{m+1}}\,\|w\|_{1,K} \quad \forall w \in H^1(K).$$

Choosing $w = u - u_m$ in the last estimate and keeping in mind (3.5) we get

$$\|u - \Pi_K^m u\|_{0,\partial K} \lesssim \sqrt{\tfrac{h_K}{m+1}}\,\|u - u_m\|_{1,K} \lesssim \frac{h_K^{\min\{s,m\}+1/2}}{(m+1)^{s+1/2}}\,\|u\|_{s+1,K}. \tag{3.6}$$

Furthermore, due to the optimality of Π_F^m, we have

$$\|u - \Pi_F^m u\|_{0,F} \le \|u - \Pi_K^m u\|_{0,F} \le \|u - \Pi_K^m u\|_{0,\partial K},$$

which proves that estimate (3.4) follows from (3.6). □

We consider $\boldsymbol{n} \in \mathcal{P}_0(\partial\mathcal{T}_h, \mathbb{R}^d)$, where $\boldsymbol{n}|_{\partial K} = \boldsymbol{n}_K$ is the unit normal vector to ∂K oriented towards the exterior of K. Obviously, if $F = K \cap K'$ is an interior edge/face of $\mathcal{F}_h$, then $\boldsymbol{n}_K = -\boldsymbol{n}_{K'}$ on F. If $\boldsymbol{v} \in H^s(\mathcal{T}_h, \mathbb{R}^d)$ and $\boldsymbol{\tau} \in H^s(\mathcal{T}_h, \mathbb{S})$, with $s > 1/2$, the functions $\boldsymbol{v}|_{\partial\mathcal{T}_h} \in L^2(\partial\mathcal{T}_h, \mathbb{R}^d)$ and $(\boldsymbol{\tau}|_{\partial\mathcal{T}_h})\boldsymbol{n} \in L^2(\partial\mathcal{T}_h, \mathbb{R}^d)$ are meaningful by virtue of the trace theorem. For the same reason, if $\boldsymbol{v} \in H^1(\Omega, \mathbb{R}^d)$ then $\hat{\boldsymbol{v}} := \boldsymbol{v}|_{\mathcal{F}_h}$ is well-defined in $L^2(\mathcal{F}_h, \mathbb{R}^d)$.

For $k \ge 0$, we introduce the finite dimensional subspace of $\mathcal{H}$ given by

$$\mathcal{H}_h := \mathcal{P}_k(\mathcal{T}_h, \mathbb{S}) \times \mathcal{P}_k^V(\mathcal{T}_h, \mathbb{S}), \quad \text{where} \quad \mathcal{P}_k^V(\mathcal{T}_h, \mathbb{S}) := \{\boldsymbol{\tau} \in \mathcal{P}_k(\mathcal{T}_h, \mathbb{S}) : \ \boldsymbol{\tau}|_{\Omega_E} = \boldsymbol{0}\}.$$

It is essential to notice that, for any $\underline{\boldsymbol{\tau}} = (\boldsymbol{\tau}_E, \boldsymbol{\tau}_V) \in \mathcal{H}_h$, $\boldsymbol{\tau} = \boldsymbol{\tau}_E + \omega(\boldsymbol{x})\boldsymbol{\tau}_V$ lies in $\mathcal{P}_k(\mathcal{T}_h, \mathbb{S})$.

Lemma 3.2. *There exists a constant $C > 0$ independent of h, k, and ω such that*

$$\|\tfrac{h_F^{1/2}}{k+1}\boldsymbol{\tau}\boldsymbol{n}\|_{0,\partial\mathcal{T}_h} \le C\|\underline{\boldsymbol{\tau}}\|_{\mathcal{H}} \quad \forall \underline{\boldsymbol{\tau}} = (\boldsymbol{\tau}_E, \boldsymbol{\tau}_V) \in \mathcal{H}_h \quad \textit{with } \boldsymbol{\tau} = \boldsymbol{\tau}_E + \omega\boldsymbol{\tau}_V. \tag{3.7}$$

Proof. According to (3.2), there exists $c > 0$ independent of h and k such that

$$\tfrac{h_K^{1/2}}{k+1}\|v\|_{0,\partial K} \le c\|v\|_{0,K} \quad \forall v \in \mathcal{P}_k(K).$$

Applying this discrete trace inequality componentwise we deduce that

$$\|\tfrac{h_F^{1/2}}{k+1}\boldsymbol{\tau}\boldsymbol{n}\|_{0,\partial\mathcal{T}_h}^2 = \sum_{K\in\mathcal{T}_h} \tfrac{h_F}{(k+1)^2}\|\boldsymbol{\tau}\boldsymbol{n}_K\|_{0,\partial K}^2 \lesssim \sum_{K\in\mathcal{T}_h} \tfrac{h_K}{(k+1)^2}\|\boldsymbol{\tau}\|_{0,\partial K}^2 \lesssim \sum_{K\in\mathcal{T}_h} \|\boldsymbol{\tau}_E + \omega\boldsymbol{\tau}_V\|_{0,K}^2,$$

for all $\underline{\boldsymbol{\tau}} = (\boldsymbol{\tau}_E, \boldsymbol{\tau}_V) \in \mathcal{H}_h$, and the result follows from the triangle inequality and (2.5). □

In the sequel, we will continue to use the notation $\Pi_{\mathcal{T}}^m$ to refer to the L^2-orthogonal projection onto $\mathcal{P}_m(\mathcal{T}_h, E)$, for $E \in \{\mathbb{R}^d, \mathbb{S}\}$. It is important to notice that the tensorial version of $\Pi_{\mathcal{T}}^m$ preserves naturally the symmetry of matrices since it is obtained by applying the scalar operator componentwise. Similarly, $\Pi_{\mathcal{F}}^m$ will denote indistinctly the L^2-orthogonal projection onto $\mathcal{P}_m(\mathcal{F}_h)$ and $\mathcal{P}_m(\mathcal{F}_h, \mathbb{R}^d)$. We let $\underline{\Pi}_{\mathcal{T}}^k : \mathcal{H} \to \mathcal{H}_h$ the projection defined by $\underline{\Pi}_{\mathcal{T}}^k\underline{\boldsymbol{\tau}} := (\Pi_{\mathcal{T}}^k\boldsymbol{\tau}_E, \Pi_{\mathcal{T}}^k\boldsymbol{\tau}_V)$ for all $\underline{\boldsymbol{\tau}} = (\boldsymbol{\tau}_E, \boldsymbol{\tau}_V) \in \mathcal{H}$.

Lemma 3.3. *There exists a constant $C > 0$ independent of h, k and ω such that*

$$\|\underline{\boldsymbol{\tau}} - \underline{\Pi}_{\mathcal{T}}^k\underline{\boldsymbol{\tau}}\|_{\mathcal{H}} + \|\tfrac{h_F^{1/2}}{k+1}(\boldsymbol{\tau} - \Pi_{\mathcal{T}}^k\boldsymbol{\tau})\boldsymbol{n}\|_{0,\partial\mathcal{T}_h} \le C\,\frac{h_K^{\min\{r,k\}+1}}{(k+1)^{r+1}}\Big(\sum_{j=1}^{J}\|\boldsymbol{\tau}_E\|_{1+r,\Omega_j}^2 + \omega_j^2\|\boldsymbol{\tau}_V\|_{1+r,\Omega_j}^2\Big)^{1/2}, \tag{3.8}$$

for all $\underline{\boldsymbol{\tau}} = (\boldsymbol{\tau}_E, \boldsymbol{\tau}_V) \in \mathcal{H}$ such that $\boldsymbol{\tau}_E \in H^{1+r}(\cup_j\Omega_j, \mathbb{S})$ and $\boldsymbol{\tau}_V \in H^{1+r}(\cup_j\Omega_j, \mathbb{S})$, with $r \ge 0$.

Proof. Given $K \in \mathcal{T}_h(\Omega_j)$, $1 \le j \le J$, we obtain from (3.3) that

$$\|\boldsymbol{\tau}_E - \Pi_K^k\boldsymbol{\tau}_E\|_{0,K}^2 + \omega_j^2\|\boldsymbol{\tau}_V - \Pi_K^k\boldsymbol{\tau}_V\|_{0,K}^2 \lesssim \frac{h_K^{2\min\{r,k\}+2}}{(k+1)^{2r+2}}(\|\boldsymbol{\tau}_E\|_{1+r,K}^2 + \omega_j^2\|\boldsymbol{\tau}_V\|_{1+r,K}^2).$$

Moreover, applying (3.4) gives

$$\tfrac{h_K}{(k+1)^2}\|(\boldsymbol{\tau} - \Pi_K^k\boldsymbol{\tau})\boldsymbol{n}_K\|_{0,\partial K}^2 \lesssim \frac{h_K^{2\min\{r,k\}+2}}{(k+1)^{2r+3}}\|\boldsymbol{\tau}\|_{1+r,K}^2 \lesssim \frac{h_K^{2\min\{r,k\}+2}}{(k+1)^{2r+2}}(\|\boldsymbol{\tau}_E\|_{1+r,K}^2 + \omega_j^2\|\boldsymbol{\tau}_V\|_{1+r,K}^2).$$

The result is obtained by first summing the last two estimates over all elements K in the mesh $\mathcal{T}_h(\Omega_j)$, and then summing over all subdomains Ω_j for j ranging from 1 to J. □

In what follows, given $\underline{\boldsymbol{v}} := (\boldsymbol{v}, \hat{\boldsymbol{v}}) \in H^s(\mathcal{T}_h, \mathbb{R}^d) \times L^2(\mathcal{F}_h, \mathbb{R}^d)$, with $s > 1/2$, we define $[\![\underline{\boldsymbol{v}}]\!] \in L^2(\partial\mathcal{T}_h, \mathbb{R}^d)$ by

$$[\![\underline{\boldsymbol{v}}]\!]|_{\partial K} := \boldsymbol{v}|_{\partial K} - \hat{\boldsymbol{v}}|_{\partial K} \quad \forall K \in \mathcal{T}_h.$$

We introduce the space $\mathcal{V} := H_0^1(\mathcal{T}_h,\mathbb{R}^d)\times L^2(\mathcal{F}_h^0,\mathbb{R}^d)$, where

$$L^2(\mathcal{F}_h^0,\mathbb{R}^d) := \{\boldsymbol{v}\in L^2(\mathcal{F}_h,\mathbb{R}^d);\ \boldsymbol{v}|_F = \mathbf{0},\ \forall F\in\mathcal{F}_h^\partial\},$$

and endowed it with the semi-norm

$$\|\underline{\boldsymbol{v}}\|_{\mathcal{V}}^2 = \|\nabla\boldsymbol{v}\|_{0,\mathcal{T}_h}^2 + \|\frac{k+1}{h_{\mathcal{F}}^{1/2}}[\![\underline{\boldsymbol{v}}]\!]\|_{0,\partial\mathcal{T}_h}^2 \quad \forall\underline{\boldsymbol{v}} := (\boldsymbol{v},\hat{\boldsymbol{v}})\in\mathcal{V}, \tag{3.9}$$

where $h_{\mathcal{F}}\in\mathcal{P}_0(\mathcal{F}_h)$ is given by $h_{\mathcal{F}}|_F := h_F$ for all $F\in\mathcal{F}_h$. For $k\geq 0$, we consider the finite dimensional subspace $\mathcal{V}_h := \mathcal{P}_{k+1}(\mathcal{T}_h,\mathbb{R}^d)\times\mathcal{P}_{k+1}(\mathcal{F}_h^0,\mathbb{R}^d)$ of $\mathcal{V}$, where

$$\mathcal{P}_{k+1}(\mathcal{F}_h^0,\mathbb{R}^d) := \{\hat{\boldsymbol{v}}\in\mathcal{P}_{k+1}(\mathcal{F}_h,\mathbb{R}^d);\ \hat{\boldsymbol{v}}|_F = \mathbf{0},\ \forall F\in\mathcal{F}_h^\partial\}.$$

We introduce the operator $\underline{\Xi}_h^{k+1}:\ \mathcal{V}\to\mathcal{V}_h$ given by $\underline{\Xi}_h^{k+1}\underline{\boldsymbol{v}} = (\Pi_{\mathcal{T}}^{k+1}\boldsymbol{v},\Pi_{\mathcal{F}}^{k+1}\hat{\boldsymbol{v}})$, for all $\underline{\boldsymbol{v}} = (\boldsymbol{v},\hat{\boldsymbol{v}})\in\mathcal{V}$. Moreover, we consider the linear operator $\underline{i}:\ H_0^1(\Omega,\mathbb{R}^d)\to\mathcal{V}$ defined, for any $\boldsymbol{v}\in H_0^1(\Omega,\mathbb{R}^d)$, by

$$\underline{i}(\boldsymbol{v}) := (\boldsymbol{v},\hat{\boldsymbol{v}})\in\mathcal{V},\quad \text{with } \hat{\boldsymbol{v}} := \boldsymbol{v}|_{\mathcal{F}_h}.$$

We point out that $[\![\underline{i}(\boldsymbol{v})]\!] = \mathbf{0}$ for all $\boldsymbol{v}\in H_0^1(\Omega,\mathbb{R}^d)$.

Lemma 3.4. *There exists a constant $C>0$ independent of h and k such that*

$$\|\underline{i}(\boldsymbol{u}) - \underline{\Xi}_h^{k+1}\underline{i}(\boldsymbol{u})\|_{\mathcal{V}} \leq C\frac{h^{\min\{r,k\}+1}}{(k+1)^{r+1/2}}\Big(\sum_{j=1}^J\|\boldsymbol{u}\|_{2+r,\Omega_j}^2\Big)^{1/2}, \tag{3.10}$$

for all $\boldsymbol{u}\in H_0^1(\Omega,\mathbb{R}^d)\cap H^{2+r}(\cup_j\Omega_j,\mathbb{R}^d)$, $r\geq 0$.

Proof. By definition, we have that

$$\|\underline{i}(\boldsymbol{u}) - \underline{\Xi}_h^{k+1}\underline{i}(\boldsymbol{u})\|_{\mathcal{V}}^2 = \sum_{K\in\mathcal{T}_h}\|\nabla(\boldsymbol{u}-\Pi_K^{k+1}\boldsymbol{u})\|_{0,K}^2 + \|\frac{k+1}{h_F^{1/2}}[\![\underline{i}(\boldsymbol{u}) - \underline{\Xi}_h^{k+1}\underline{i}(\boldsymbol{u})]\!]\|_{0,\partial K}^2$$

and it follows directly from (3.3) that

$$\|\nabla(\boldsymbol{u}-\Pi_K^{k+1}\boldsymbol{u})\|_{0,K} \lesssim \frac{h_K^{\min\{r,k\}+1}}{(k+1)^{r+1/2}}\|\boldsymbol{u}\|_{2+r,K}\quad\forall K\in\mathcal{T}_h. \tag{3.11}$$

On the other hand, using in the triangle inequality and (3.1) we get

$$\|\frac{k+1}{h_F^{1/2}}[\![\underline{i}(\boldsymbol{u}) - \underline{\Xi}_h^{k+1}\underline{i}(\boldsymbol{u})]\!]\|_{0,\partial K} \lesssim \frac{k+1}{h_K^{1/2}}\|\boldsymbol{u}-\Pi_K^{k+1}\boldsymbol{u}\|_{0,\partial K} + \sum_{F\in\mathcal{F}(K)}\frac{k+1}{h_K^{1/2}}\|\boldsymbol{u}-\Pi_F^{k+1}\boldsymbol{u}\|_{0,F},$$

and it follows from (3.4) that

$$\|\frac{k+1}{h_F^{1/2}}[\![\underline{i}(\boldsymbol{u}) - \underline{\Xi}_h^{k+1}\underline{i}(\boldsymbol{u})]\!]\|_{0,\partial K} \lesssim \frac{h_K^{\min\{r,k\}+1}}{(k+1)^{r+1/2}}\|\boldsymbol{u}\|_{2+r,K}\quad\forall K\in\mathcal{T}_h. \tag{3.12}$$

Summing (3.11) and (3.12) over $K\in\mathcal{T}_h(\Omega_j)$ and then over $j=1,\dots,J$ gives the result. □

4. The HDG semi-discrete scheme and its convergence analysis

For all $\underline{\boldsymbol{\tau}}\in\mathcal{H}$ such that $\boldsymbol{\tau} = \boldsymbol{\tau}_E + \omega\boldsymbol{\tau}_V\in H^s(\mathcal{T}_h,\mathbb{S})$, $s\geq 1/2$, and for all $\underline{\boldsymbol{v}}\in\mathcal{V}$, we introduce the bilinear form defined by:

$$B_h(\underline{\boldsymbol{\tau}},\underline{\boldsymbol{v}}) := (\boldsymbol{\tau},\boldsymbol{\varepsilon}(\boldsymbol{v}))_{\mathcal{T}_h} - \langle\boldsymbol{\tau}\boldsymbol{n},[\![\underline{\boldsymbol{v}}]\!]\rangle_{\partial\mathcal{T}_h}.$$

Applying the Cauchy–Schwarz inequality and (2.5), we deduce that

$$|B_h(\underline{\boldsymbol{\tau}},\underline{\boldsymbol{v}})| \lesssim (\|\underline{\boldsymbol{\tau}}\|_{\mathcal{H}}^2 + \|\frac{h_{\mathcal{F}}^{1/2}}{k+1}\boldsymbol{\tau}\boldsymbol{n}\|_{0,\partial\mathcal{T}_h}^2)^{1/2}\|\underline{\boldsymbol{v}}\|_{\mathcal{V}}. \tag{4.1}$$

Combining this estimate with the inverse inequality (3.7) we deduce that there exists a constant $C>0$ independent of h, k, and ω such that

$$|B_h(\underline{\boldsymbol{\tau}},\underline{\boldsymbol{v}})| \leq C\|\underline{\boldsymbol{\tau}}\|_{\mathcal{H}}\|\underline{\boldsymbol{v}}\|_{\mathcal{V}}\quad\text{for all } \underline{\boldsymbol{\tau}}\in\mathcal{H}_h \text{ and } \underline{\boldsymbol{v}}\in\mathcal{V}. \tag{4.2}$$

We propose the following HDG space discretization method for problem (2.9): find $\underline{\boldsymbol{\sigma}}_h := (\boldsymbol{\sigma}_{E,h},\boldsymbol{\sigma}_{V,h})\in C^1_{[0,T]}(\mathcal{H}_h)$ and $\underline{\boldsymbol{u}}_h := (\boldsymbol{u}_h,\hat{\boldsymbol{u}}_h)\in C^1_{[0,T]}(\mathcal{V}_h)$ satisfying

$$\begin{aligned}&(\dot{\underline{\boldsymbol{\sigma}}}_h,\underline{\boldsymbol{\tau}})_{\mathcal{H}} + (\rho\dot{\boldsymbol{u}}_h,\boldsymbol{v})_{\mathcal{T}_h} + (\mathcal{G}\boldsymbol{\sigma}_{V,h},\omega\boldsymbol{\tau}_V)_{\mathcal{T}_h}\\ &\qquad + B_h(\underline{\boldsymbol{\sigma}}_h,\underline{\boldsymbol{v}}) - B_h(\underline{\boldsymbol{\tau}},\underline{\boldsymbol{u}}_h) + \langle\frac{(k+1)^2}{h_{\mathcal{F}}}[\![\underline{\boldsymbol{u}}_h]\!],[\![\underline{\boldsymbol{v}}]\!]\rangle_{\partial\mathcal{T}_h} = (\boldsymbol{f}(t),\boldsymbol{v})_{\mathcal{T}_h}\end{aligned} \tag{4.3}$$

for all $\underline{\boldsymbol{\tau}} = (\boldsymbol{\tau}_E,\boldsymbol{\tau}_V)\in\mathcal{H}_h$ and $\underline{\boldsymbol{v}} = (\boldsymbol{v},\hat{\boldsymbol{v}})\in\mathcal{V}_h$. We start up problem (4.3) with the initial conditions

$$\underline{\boldsymbol{\sigma}}_h(0) = \underline{\Pi}_{\mathcal{T}}^k(\boldsymbol{\sigma}_E^0,\boldsymbol{\sigma}_V^0),\quad \boldsymbol{u}_h(0) = \Pi_{\mathcal{T}}^{k+1}\boldsymbol{d}^1. \tag{4.4}$$

Proposition 4.1. *Problem (4.3) admits a unique solution.*

Proof. The algebraic differential equation (4.3) can be written as follows

$$\begin{aligned}(\underline{\dot{\boldsymbol{\sigma}}}_h,\underline{\boldsymbol{\tau}})_{\mathcal{H}}+(\rho\dot{\boldsymbol{u}}_h,\boldsymbol{v})_{\mathcal{T}_h}+(\mathcal{G}\boldsymbol{\sigma}_{V,h},\omega\boldsymbol{\tau}_V)_{\mathcal{T}_h}+(\boldsymbol{\sigma}_h,\boldsymbol{\varepsilon}(\boldsymbol{v}))_{\mathcal{T}_h}-(\boldsymbol{\tau},\boldsymbol{\varepsilon}(\boldsymbol{u}_h))_{\mathcal{T}_h}-\langle\boldsymbol{\sigma}_h\boldsymbol{n},\boldsymbol{v}\rangle_{\partial\mathcal{T}_h}\\ +\langle[\![\underline{\boldsymbol{u}}_h]\!],\tfrac{(k+1)^2}{h_F}\boldsymbol{v}+\boldsymbol{\tau}\boldsymbol{n}\rangle_{\partial\mathcal{T}_h}=(\boldsymbol{f}(t),\boldsymbol{v})_{\mathcal{T}_h}\quad\forall\underline{\boldsymbol{\tau}}\in\mathcal{H}_h,\ \forall\boldsymbol{v}\in\mathcal{P}_{k+1}(\mathcal{T}_h,\mathbb{R}^d)\\ \langle\tfrac{(k+1)^2}{h_F}\hat{\boldsymbol{u}}_h,\hat{\boldsymbol{v}}\rangle_{\partial\mathcal{T}_h}=\langle\tfrac{(k+1)^2}{h_F}\boldsymbol{u}_h-\boldsymbol{\sigma}_h\boldsymbol{n},\hat{\boldsymbol{v}}\rangle_{\partial\mathcal{T}_h}\quad\forall\hat{\boldsymbol{v}}\in\mathcal{P}_{k+1}(\mathcal{F}_h^0,\mathbb{R}^d).\end{aligned}\tag{4.5}$$

It follows from the second equation of (4.5), that for all $t\in(0,T]$, $\hat{\boldsymbol{u}}_h(t)$ can be expressed as follows:

$$\hat{\boldsymbol{u}}_h(t)=\{\{\boldsymbol{u}_h\}\}(t)-\tfrac{h_F}{(k+1)^2}\{\{\boldsymbol{\sigma}_h\boldsymbol{n}\}\}(t)$$

where $\{\{\boldsymbol{u}_h\}\}(t)$ and $\{\{\boldsymbol{\sigma}_h\boldsymbol{n}\}\}(t)$ are defined in $\mathcal{P}_{k+1}(\mathcal{F}_h^0,\mathbb{R}^d)$ by $\{\{\boldsymbol{u}_h\}\}|_F:=\frac{1}{2}(\boldsymbol{u}_h|_K+\boldsymbol{u}_h|_{K'})|_F$ and $\{\{\boldsymbol{\sigma}_h\boldsymbol{n}\}\}|_F:=\frac{1}{2}(\boldsymbol{\sigma}_h|_K\boldsymbol{n}_K+\boldsymbol{\sigma}_h|_{K'}\boldsymbol{n}_{K'})|_F$, respectively, for all $F\in\mathcal{F}_h^0$ with $F=K\cap K'$. We can then eliminate $\hat{\boldsymbol{u}}_h$ and end up with the system of ordinary differential equations

$$\begin{aligned}(\underline{\dot{\boldsymbol{\sigma}}}_h,\underline{\boldsymbol{\tau}})_{\mathcal{H}}+(\rho\dot{\boldsymbol{u}}_h,\boldsymbol{v})_{\mathcal{T}_h}+(\mathcal{G}\boldsymbol{\sigma}_{V,h},\omega\boldsymbol{\tau}_V)_{\mathcal{T}_h}+(\boldsymbol{\sigma}_h,\boldsymbol{\varepsilon}(\boldsymbol{v}))_{\mathcal{T}_h}-(\boldsymbol{\tau},\boldsymbol{\varepsilon}(\boldsymbol{u}_h))_{\mathcal{T}_h}-\langle\boldsymbol{\sigma}_h\boldsymbol{n},\boldsymbol{v}\rangle_{\partial\mathcal{T}_h}\\ +\langle\boldsymbol{u}_h-(\{\boldsymbol{u}_h\}-\tfrac{h_F}{(k+1)^2}\{\boldsymbol{\sigma}_h\boldsymbol{n}\}),\tfrac{(k+1)^2}{h_F}\boldsymbol{v}+\boldsymbol{\tau}\boldsymbol{n}\rangle_{\partial\mathcal{T}_h}=(\boldsymbol{f}(t),\boldsymbol{v})_{\mathcal{T}_h}\quad\forall\underline{\boldsymbol{\tau}}\in\mathcal{H}_h,\ \forall\boldsymbol{v}\in\mathcal{P}_{k+1}(\mathcal{T}_h,\mathbb{R}^d),\end{aligned}\tag{4.6}$$

with the initial conditions (4.4). We observe that $(\cdot,\cdot)_{\mathcal{H}}$ and $(\rho\cdot,\cdot)_{\mathcal{T}_h}$ are inner products in the finite dimensional function spaces $\mathcal{H}_h$ and $\mathcal{P}_{k+1}(\mathcal{T}_h,\mathbb{R}^d)$, respectively. By selecting a suitable set of basis functions for these function spaces, we can represent the semidiscrete problem (4.6) as a conventional first-order system of differential equations. As a result, the solution to (4.3) exists and is unique. □

Let us verify now that the HDG scheme (4.3) is consistent with problem (2.9).

Proposition 4.2. *Let*

$$\underline{\boldsymbol{\sigma}}:=(\boldsymbol{\sigma}_E,\boldsymbol{\sigma}_V)\in H^1_{[0,T]}(\mathcal{X}^+)\cap C^1_{[0,T]}(\mathcal{H})\quad\text{and}\quad\boldsymbol{u}\in C^1_{[0,T]}(L^2(\Omega,\mathbb{R}^d))\cap C^0_{[0,T]}(H^1_0(\Omega,\mathbb{R}^d))$$

be the solutions of (2.9) and assume that the stress tensor $\boldsymbol{\sigma}=\boldsymbol{\sigma}_E+\omega\boldsymbol{\sigma}_V$ belongs to $C^0_{[0,T]}(H^s(\mathcal{T}_h,\mathbb{S})\cap H(\mathbf{div},\Omega,\mathbb{S}))$, with $s>1/2$. Then, it holds true that

$$\begin{aligned}&(\underline{\dot{\boldsymbol{\sigma}}},\underline{\boldsymbol{\tau}})_{\mathcal{H}}+(\rho\dot{\boldsymbol{u}},\boldsymbol{v})_{\mathcal{T}_h}+(\mathcal{G}\boldsymbol{\sigma}_V,\omega\boldsymbol{\tau}_V)_{\mathcal{T}_h}\\ &\quad+B_h(\underline{\boldsymbol{\sigma}},\underline{\boldsymbol{v}})-B_h(\underline{\boldsymbol{\tau}},\underline{i}(\boldsymbol{u}))+\langle\tfrac{(k+1)^2}{h_F}[\![\underline{i}(\boldsymbol{u})]\!],[\![\underline{\boldsymbol{v}}]\!]\rangle_{\partial\mathcal{T}_h}=(\boldsymbol{f}(t),\boldsymbol{v})_{\mathcal{T}_h}\end{aligned}\tag{4.7}$$

for all $\underline{\boldsymbol{\tau}}=(\boldsymbol{\tau}_E,\boldsymbol{\tau}_V)\in\mathcal{H}_h$ and $\underline{\boldsymbol{v}}=(\boldsymbol{v},\hat{\boldsymbol{v}})\in\mathcal{V}_h$.

Proof. We point out that, as $[\![\underline{i}(\boldsymbol{u})]\!]=\mathbf{0}$, we have that

$$B_h(\underline{\boldsymbol{\tau}},\underline{i}(\boldsymbol{u}))=(\boldsymbol{\tau},\boldsymbol{\varepsilon}(\boldsymbol{u}))_{\mathcal{T}_h}\quad\forall\underline{\boldsymbol{\tau}}\in\mathcal{H}_h.$$

Moreover, the continuity of the normal components of $\boldsymbol{\sigma}$ across the interelements of $\mathcal{T}_h$ gives

$$B_h(\underline{\boldsymbol{\sigma}},\underline{\boldsymbol{v}})=(\boldsymbol{\sigma},\boldsymbol{\varepsilon}(\boldsymbol{v}))_{\mathcal{T}_h}-\langle\boldsymbol{\sigma}\boldsymbol{n},[\![\underline{\boldsymbol{v}}]\!]\rangle_{\partial\mathcal{T}_h}=(\boldsymbol{\sigma},\nabla\boldsymbol{v})_{\mathcal{T}_h}-\langle\boldsymbol{\sigma}\boldsymbol{n},\boldsymbol{v}\rangle_{\partial\mathcal{T}_h}\quad\forall\underline{\boldsymbol{v}}=(\boldsymbol{v},\hat{\boldsymbol{v}})\in\mathcal{V}_h.\tag{4.8}$$

Applying now an elementwise integration by parts to the right-hand side of the last identity followed by the substitution $\mathbf{div}\,\boldsymbol{\sigma}=\rho\dot{\boldsymbol{u}}-\boldsymbol{f}$ yields

$$B_h(\underline{\boldsymbol{\sigma}},\underline{\boldsymbol{v}})=-(\mathbf{div}\,\boldsymbol{\sigma},\boldsymbol{v})_{\mathcal{T}_h}=-(\rho\dot{\boldsymbol{u}},\boldsymbol{v})_{\mathcal{T}_h}+(\boldsymbol{f}(t),\boldsymbol{v})_{\Omega}.\tag{4.9}$$

By virtue of (4.8) and (4.9), it holds true that

$$\begin{aligned}&(\underline{\dot{\boldsymbol{\sigma}}},\underline{\boldsymbol{\tau}})_{\mathcal{H}}+(\rho\dot{\boldsymbol{u}},\boldsymbol{v})_{\mathcal{T}_h}+(\mathcal{G}\boldsymbol{\sigma}_V,\omega\boldsymbol{\tau}_V)_{\mathcal{T}_h}+B_h(\underline{\boldsymbol{\sigma}},\underline{\boldsymbol{v}})-B_h(\underline{\boldsymbol{\tau}},\underline{i}(\boldsymbol{u}))+\langle\tfrac{(k+1)^2}{h_F}[\![\underline{i}(\boldsymbol{u})]\!],[\![\underline{\boldsymbol{v}}]\!]\rangle_{\partial\mathcal{T}_h}\\ &\quad=(\underline{\dot{\boldsymbol{\sigma}}},\underline{\boldsymbol{\tau}})_{\mathcal{H}}+(\mathcal{G}\boldsymbol{\sigma}_V,\omega\boldsymbol{\tau}_V)_{\mathcal{T}_h}-(\boldsymbol{\tau},\boldsymbol{\varepsilon}(\boldsymbol{u}))_{\mathcal{T}_h}+(\boldsymbol{f},\boldsymbol{v})_{\mathcal{T}_h},\end{aligned}\tag{4.10}$$

for all $\underline{\boldsymbol{\tau}}=(\boldsymbol{\tau}_E,\boldsymbol{\tau}_V)\in\mathcal{H}_h$ and $\underline{\boldsymbol{v}}=(\boldsymbol{v},\hat{\boldsymbol{v}})\in\mathcal{V}_h$. Moreover, applying Green's formula (1.2) in the second equation of (2.9) and keeping in mind the density of the embedding $\mathcal{X}^+\hookrightarrow\mathcal{H}$ we obtain

$$(\underline{\dot{\boldsymbol{\sigma}}},\underline{\boldsymbol{\tau}})_{\mathcal{H}}+(\mathcal{G}\boldsymbol{\sigma}_V,\omega\boldsymbol{\tau}_V)_{\Omega}=(\boldsymbol{\varepsilon}(\boldsymbol{u}),\boldsymbol{\tau})_{\Omega}\quad\forall\underline{\boldsymbol{\tau}}=(\boldsymbol{\tau}_E,\boldsymbol{\tau}_V)\in\mathcal{H}.$$

Substituting back this identity in (4.10) gives the result. □

We begin now the convergence analysis of the HDG method (4.3) by considering the splitting $\underline{\boldsymbol{\sigma}}(t)-\underline{\boldsymbol{\sigma}}_h(t)=\underline{\boldsymbol{\chi}}(t)+\underline{\boldsymbol{\pi}}_h(t)$ of the error in the stress variable with $\underline{\boldsymbol{\chi}}(t)=\underline{\boldsymbol{\sigma}}(t)-\underline{\Pi}^k_{\mathcal{T}}\underline{\boldsymbol{\sigma}}(t)$ and $\underline{\boldsymbol{\pi}}_h(t)=\underline{\Pi}^k_{\mathcal{T}}\underline{\boldsymbol{\sigma}}(t)-\underline{\boldsymbol{\sigma}}_h(t)$. Likewise, we introduce the decomposition $\underline{i}(\boldsymbol{u}(t))-\underline{\boldsymbol{u}}_h(t)=\underline{\boldsymbol{q}}(t)+\underline{\boldsymbol{e}}_h(t)$ of the error in the velocity variable with $\underline{\boldsymbol{q}}(t)=\underline{i}(\boldsymbol{u}(t))-\underline{\Xi}^{k+1}_{\mathcal{T}}\underline{i}(\boldsymbol{u}(t))$, and $\underline{\boldsymbol{e}}_h(t)=\underline{\Xi}^{k+1}_{\mathcal{T}}\underline{i}(\boldsymbol{u}(t))-\underline{\boldsymbol{u}}_h(t)$. Hence, the components of the projected errors $\underline{\boldsymbol{\pi}}_h:=(\boldsymbol{\pi}_{E,h},\boldsymbol{\pi}_{V,h})\in C^1(\mathcal{H}_h)$ and $\underline{\boldsymbol{e}}_h:=(\boldsymbol{e}_h,\hat{\boldsymbol{e}}_h)\in C^1(\mathcal{V}_h)$ are given by

$$\boldsymbol{\pi}_{E,h}=\Pi^k_{\mathcal{T}}\boldsymbol{\sigma}_E-\boldsymbol{\sigma}_{E,h},\quad\boldsymbol{\pi}_{V,h}=\Pi^k_{\mathcal{T}}\boldsymbol{\sigma}_V-\boldsymbol{\sigma}_{V,h}\quad\text{and}\quad\boldsymbol{e}_h=\Pi^{k+1}_{\mathcal{T}}\boldsymbol{u}-\boldsymbol{u}_h,\quad\hat{\boldsymbol{e}}_h=\Pi^{k+1}_{\mathcal{F}}\hat{\boldsymbol{u}}-\hat{\boldsymbol{u}}_h,$$

where we recall that $\hat{\boldsymbol{u}} = \boldsymbol{u}|_{\mathcal{F}_h}$. We also have that $\underline{\chi} = (\chi_E, \chi_V)$ and $\underline{\boldsymbol{q}} = (\boldsymbol{q}, \hat{\boldsymbol{q}})$ with

$$\chi_E = \boldsymbol{\sigma}_E - \Pi_{\mathcal{T}}^k \boldsymbol{\sigma}_E, \quad \chi_V = \boldsymbol{\sigma}_V - \Pi_{\mathcal{T}}^k \boldsymbol{\sigma}_V \quad \text{and} \quad \boldsymbol{q} = \boldsymbol{u} - \Pi_{\mathcal{T}}^{k+1} \boldsymbol{u}, \quad \hat{\boldsymbol{q}} = \hat{\boldsymbol{u}} - \Pi_{\mathcal{F}}^{k+1} \hat{\boldsymbol{u}}.$$

Moreover, we will write $\boldsymbol{\pi}_h := \boldsymbol{\pi}_{E,h} + \omega \boldsymbol{\pi}_{V,h}$ and $\chi := \chi_E + \omega \chi_V$.

Lemma 4.1. *Under the conditions of Proposition 4.2, there exists a constant $C > 0$ independent of h, k and ω such that*

$$\max_{[0,T]} \|\underline{\boldsymbol{\pi}}_h(t)\|_{\mathcal{H}}^2 + \max_{[0,T]} \|\boldsymbol{e}_h(t)\|_{0,\mathcal{T}_h}^2 + \int_0^T \|\tfrac{k+1}{h_{\mathcal{F}}^{1/2}} [\![\underline{\boldsymbol{e}}_h]\!]\|_{0,\partial\mathcal{T}_h}^2 \mathrm{d}t \le C \int_0^T \Big(\|\underline{\boldsymbol{q}}\|_{\mathcal{V}_h}^2 + \|\tfrac{h_{\mathcal{F}}^{1/2}}{k+1} \chi \boldsymbol{n}\|_{0,\partial\mathcal{T}_h}^2 \Big) \mathrm{d}t. \tag{4.11}$$

Proof. Using the consistency property (4.7) it is straightforward that

$$\begin{aligned}
(\dot{\underline{\boldsymbol{\pi}}}_h, \underline{\boldsymbol{\tau}})_{\mathcal{H}} + (\rho \dot{\boldsymbol{e}}_h, \boldsymbol{v})_{\mathcal{T}_h} + (\mathcal{G} \boldsymbol{\pi}_{V,h}, \omega \boldsymbol{\tau}_V)_{\mathcal{T}_h} + B_h(\underline{\boldsymbol{\pi}}_h, \underline{\boldsymbol{v}}) - B_h(\underline{\boldsymbol{\tau}}, \underline{\boldsymbol{e}}_h) + \langle \tfrac{(k+1)^2}{h_{\mathcal{F}}} [\![\underline{\boldsymbol{e}}_h]\!], [\![\underline{\boldsymbol{v}}]\!] \rangle_{\partial\mathcal{T}_h} \\
= -(\dot{\underline{\chi}}, \underline{\boldsymbol{\tau}})_{\mathcal{H}} - (\rho \dot{\boldsymbol{q}}, \boldsymbol{v})_{\mathcal{T}_h} - (\mathcal{G} \chi_V, \omega \boldsymbol{\tau}_V)_{\mathcal{T}_h} - B_h(\underline{\chi}, \underline{\boldsymbol{v}}) + B_h(\underline{\boldsymbol{\tau}}, \underline{\boldsymbol{q}}) - \langle \tfrac{(k+1)^2}{h_{\mathcal{F}}} [\![\underline{\chi}]\!], [\![\underline{\boldsymbol{v}}]\!] \rangle_{\partial\mathcal{T}_h} \\
= \langle \chi \boldsymbol{n}, [\![\underline{\boldsymbol{v}}]\!] \rangle_{\partial\mathcal{T}_h} + B_h(\underline{\boldsymbol{\tau}}, \underline{\boldsymbol{q}}) - \langle \tfrac{(k+1)^2}{h_{\mathcal{F}}} [\![\underline{\boldsymbol{q}}]\!], [\![\underline{\boldsymbol{v}}]\!] \rangle_{\partial\mathcal{T}_h}
\end{aligned} \tag{4.12}$$

for all $\underline{\boldsymbol{\tau}} = (\boldsymbol{\tau}_E, \boldsymbol{\tau}_V) \in \mathcal{H}_h$ and $\underline{\boldsymbol{v}} = (\boldsymbol{v}, \hat{\boldsymbol{v}}) \in \mathcal{V}_h$. The last identity follows from orthogonal properties and from the fact that the coefficient parameters are piecewise constant. Indeed, taking into account that $\mathcal{A}(\boldsymbol{x}) \mathcal{P}_k(\mathcal{T}_h, \mathbb{S}) \subset \mathcal{P}_k(\mathcal{T}_h, \mathbb{S})$, $\mathcal{G}(\boldsymbol{x}) \mathcal{P}_k(\mathcal{T}_h, \mathbb{S}) \subset \mathcal{P}_k(\mathcal{T}_h, \mathbb{S})$, and $\omega(\boldsymbol{x}) \mathcal{P}_k(\mathcal{T}_h, \mathbb{S}) \subset \mathcal{P}_k(\mathcal{T}_h, \mathbb{S})$ we deduce that

$$\begin{aligned}
(\dot{\underline{\chi}}, \underline{\boldsymbol{\tau}})_{\mathcal{H}} + (\mathcal{G} \chi_V, \omega \boldsymbol{\tau}_V)_{\mathcal{T}_h} = (\dot{\boldsymbol{\sigma}}_E - \Pi_{\mathcal{T}}^k \dot{\boldsymbol{\sigma}}_E, \mathcal{A} \boldsymbol{\tau}_E) + (\dot{\boldsymbol{\sigma}}_V - \Pi_{\mathcal{T}}^k \dot{\boldsymbol{\sigma}}_V, \omega^2 \mathcal{G} \boldsymbol{\tau}_V) \\
+ (\boldsymbol{\sigma}_V - \Pi_{\mathcal{T}}^k \boldsymbol{\sigma}_V, \omega \mathcal{G} \boldsymbol{\tau}_V)_{\mathcal{T}_h} = 0 \quad \forall \underline{\boldsymbol{\tau}} \in \mathcal{H}_h.
\end{aligned}$$

Similarly, because $\rho(\boldsymbol{x}) \mathcal{P}_{k+1}(\mathcal{T}_h, \mathbb{R}^d) \subset \mathcal{P}_{k+1}(\mathcal{T}_h, \mathbb{R}^d)$ we also have

$$(\rho \dot{\boldsymbol{q}}, \boldsymbol{v})_{\mathcal{T}_h} = (\dot{\boldsymbol{u}} - \Pi_{\mathcal{T}}^{k+1} \dot{\boldsymbol{u}}, \rho \boldsymbol{v})_{\Omega} = 0 \quad \forall \boldsymbol{v} \in \mathcal{P}_{k+1}(\mathcal{T}_h, \mathbb{R}^d).$$

Finally, as $\boldsymbol{\epsilon}(\mathcal{P}_{k+1}(\mathcal{T}_h, \mathbb{R}^d)) \subset \mathcal{P}_k(\mathcal{T}_h, \mathbb{S})$, it turns out that

$$B_h(\underline{\chi}, \underline{\boldsymbol{v}}) = (\boldsymbol{\sigma} - \Pi_{\mathcal{T}}^k \boldsymbol{\sigma}, \boldsymbol{\epsilon}(\boldsymbol{v}))_{\mathcal{T}_h} - \langle \chi \boldsymbol{n}, [\![\underline{\boldsymbol{v}}]\!] \rangle_{\partial\mathcal{T}_h} = -\langle \chi \boldsymbol{n}, [\![\underline{\boldsymbol{v}}]\!] \rangle_{\partial\mathcal{T}_h} \quad \forall \underline{\boldsymbol{v}} \in \mathcal{V}_h.$$

Taking $\underline{\boldsymbol{\tau}} = \underline{\boldsymbol{\pi}}_h$ and $\underline{\boldsymbol{v}} = \underline{\boldsymbol{e}}_h$ in (4.12) and using the Cauchy–Schwarz inequality together with (4.2) yields

$$\begin{aligned}
\frac{1}{2} \frac{\mathrm{d}}{\mathrm{d}t} \big\{ (\underline{\boldsymbol{\pi}}_h, \underline{\boldsymbol{\pi}}_h)_{\mathcal{H}} + (\rho \boldsymbol{e}_h, \boldsymbol{e}_h)_{\mathcal{T}_h} \big\} + \|\tfrac{k+1}{h_{\mathcal{F}}^{1/2}} [\![\underline{\boldsymbol{e}}_h]\!]\|_{0,\partial\mathcal{T}_h}^2 \le \langle \chi \boldsymbol{n}, [\![\underline{\boldsymbol{e}}_h]\!] \rangle_{\partial\mathcal{T}_h} + B_h(\underline{\boldsymbol{\pi}}_h, \underline{\boldsymbol{q}}) - \langle \tfrac{(k+1)^2}{h_{\mathcal{F}}} [\![\underline{\boldsymbol{q}}]\!], [\![\underline{\boldsymbol{e}}_h]\!] \rangle_{\partial\mathcal{T}_h} \\
\le \|\tfrac{h_{\mathcal{F}}^{1/2}}{k+1} \chi \boldsymbol{n}\|_{0,\partial\mathcal{T}_h} \|\tfrac{k+1}{h_{\mathcal{F}}^{1/2}} [\![\underline{\boldsymbol{e}}_h]\!]\|_{0,\partial\mathcal{T}_h} + C \|\underline{\boldsymbol{\pi}}_h\|_{\mathcal{H}} \|\underline{\boldsymbol{q}}\|_{\mathcal{V}} + \|\tfrac{k+1}{h_{\mathcal{F}}^{1/2}} [\![\underline{\boldsymbol{q}}]\!]\|_{0,\partial\mathcal{T}_h} \|\tfrac{k+1}{h_{\mathcal{F}}^{1/2}} [\![\underline{\boldsymbol{e}}_h]\!]\|_{0,\partial\mathcal{T}_h}.
\end{aligned}$$

We notice that because of assumption (4.4), the projected errors satisfy vanishing initial conditions, namely, $\underline{\boldsymbol{\pi}}_h(0) = (\boldsymbol{0}, \boldsymbol{0})$ and $\boldsymbol{e}_h(0) = \boldsymbol{0}$. Hence, integrating over $t \in (0, T]$ and using again the Cauchy–Schwarz inequality we deduce that

$$\begin{aligned}
\|\underline{\boldsymbol{\pi}}_h(t)\|_{\mathcal{H}}^2 + \|\rho^{1/2} \boldsymbol{e}_h(t)\|_{0,\mathcal{T}_h}^2 + \int_0^t \|\tfrac{k+1}{h_{\mathcal{F}}^{1/2}} [\![\underline{\boldsymbol{e}}_h]\!]\|_{0,\partial\mathcal{T}_h}^2 \mathrm{d}s \lesssim \max_{[0,T]} \|\underline{\boldsymbol{\pi}}_h(t)\|_{\mathcal{H}} \int_0^T \|\underline{\boldsymbol{q}}\|_{\mathcal{V}} \mathrm{d}t \\
+ \Big(\int_0^T (\|\tfrac{h_{\mathcal{F}}^{1/2}}{k+1} \chi \boldsymbol{n}\|_{0,\partial\mathcal{T}_h}^2 + \|\tfrac{k+1}{h_{\mathcal{F}}^{1/2}} [\![\underline{\boldsymbol{q}}]\!]\|_{0,\partial\mathcal{T}_h}^2) \mathrm{d}t \Big)^{1/2} \Big(\int_0^T \|\tfrac{k+1}{h_{\mathcal{F}}^{1/2}} [\![\underline{\boldsymbol{e}}_h]\!]\|_{0,\partial\mathcal{T}_h}^2 \mathrm{d}t \Big)^{1/2},
\end{aligned}$$

for all $t \in (0, T]$. We conclude, by a simple application of Young's inequality, that

$$\begin{aligned}
\max_{[0,T]} \|\underline{\boldsymbol{\pi}}_h(t)\|_{\mathcal{H}}^2 + \max_{[0,T]} \|\boldsymbol{e}_h(t)\|_{0,\mathcal{T}_h}^2 + \int_0^T \|\tfrac{k+1}{h_{\mathcal{F}}^{1/2}} [\![\underline{\boldsymbol{e}}_h]\!]\|_{0,\partial\mathcal{T}_h}^2 \mathrm{d}t \\
\lesssim \int_0^T \Big(\|\tfrac{h_{\mathcal{F}}^{1/2}}{k+1} \chi \boldsymbol{n}\|_{0,\partial\mathcal{T}_h}^2 + \|\tfrac{k+1}{h_{\mathcal{F}}^{1/2}} [\![\underline{\boldsymbol{q}}]\!]\|_{0,\partial\mathcal{T}_h}^2 \Big) \mathrm{d}t + \Big(\int_0^T \|\underline{\boldsymbol{q}}\|_{\mathcal{V}} \mathrm{d}t \Big)^2,
\end{aligned}$$

and the result follows. □

Theorem 4.1. *Let*

$$\underline{\boldsymbol{\sigma}} := (\boldsymbol{\sigma}_E, \boldsymbol{\sigma}_V) \in H_{[0,T]}^1(\mathcal{X}^+) \cap C_{[0,T]}^1(\mathcal{H}) \quad \text{and} \quad \boldsymbol{u} \in C_{[0,T]}^1(L^2(\Omega, \mathbb{R}^d)) \cap C_{[0,T]}^0(H_0^1(\Omega, \mathbb{R}^d))$$

be the solutions of (2.9). Assume that $\boldsymbol{\sigma}_E, \boldsymbol{\sigma}_V \in C^0(H^{1+r}(\cup_j \Omega_j, \mathbb{S}))$ and $\boldsymbol{u} \in C^0(H^{2+r}(\cup_j \Omega_j, \mathbb{R}^d))$, with $r \ge 0$. Then, there exists a constant $C > 0$ independent of h, k, and ω such that

$$\begin{aligned}
\max_{[0,T]} \|(\underline{\boldsymbol{\sigma}} - \underline{\boldsymbol{\sigma}}_h)(t)\|_{\mathcal{H}} + \max_{[0,T]} \|(\boldsymbol{u} - \boldsymbol{u}_h)(t)\|_{0,\mathcal{T}_h} + \left(\int_0^T \|\tfrac{k+1}{h_{\mathcal{F}}^{1/2}} [\![\underline{i}(\boldsymbol{u}) - \underline{\boldsymbol{u}}_h]\!]\|_{0,\partial\mathcal{T}_h}^2 \mathrm{d}t \right)^{1/2} \\
\le C \frac{h_K^{\min\{r,k\}+1}}{(k+1)^{r+1}} \Big(\sum_{j=1}^J (\max_{[0,T]} \|\boldsymbol{\tau}_E\|_{1+r,\Omega_j}^2 + \omega_j^2 \max_{[0,T]} \|\boldsymbol{\tau}_V\|_{1+r,\Omega_j}^2 + \max_{[0,T]} \|\boldsymbol{u}\|_{2+r,\Omega_j}^2) \Big)^{1/2} \quad \forall k \ge 0.
\end{aligned}$$

Proof. It follows from the triangle inequality and (4.11) that

$$\max_{[0,T]} \|(\underline{\boldsymbol{\sigma}} - \underline{\boldsymbol{\sigma}}_h)(t)\|^2_{\mathcal{H}} + \max_{[0,T]} \|(\boldsymbol{u} - \boldsymbol{u}_h)(t)\|^2_{0,\mathcal{T}_h} + \int_0^T \| \tfrac{k+1}{h_{\mathcal{F}}^{1/2}} [\![\underline{i}(\boldsymbol{u}) - \underline{\boldsymbol{u}}_h]\!] \|^2_{0,\partial\mathcal{T}_h} \, \mathrm{d}t$$
$$\leq \max_{[0,T]} \|\chi(t)\|^2_{\mathcal{H}} + \max_{[0,T]} \|\boldsymbol{q}(t)\|^2_{0,\mathcal{T}_h} + C \int_0^T \left(\|\underline{\boldsymbol{q}}\|^2_{\mathcal{V}_h} + \| \tfrac{h_{\mathcal{F}}^{1/2}}{k+1} \chi \boldsymbol{n} \|^2_{0,\partial\mathcal{T}_h} \right) \mathrm{d}t,$$

and the result follows directly from the error estimates (3.8) and (3.10). □

Remark 4.1. The energy norm error estimates provided by Theorem 4.1 are quasi-optimal in h and suboptimal by a factor of $k^{1/2}$ in k for the stress variable. This issue has been previously addressed in the literature, as shown in [36,37], where similar bounds were obtained for stationary (scalar) second-order elliptic problems. However, the error estimate for the velocity field is currently suboptimal in h by one order, and it remains unclear how the duality argument of Aubin–Nitsche can be applied to obtain a quasi-optimal error estimate in h for this variable in the L^2-norm.

5. The fully discrete scheme and its convergence analysis

Given $L \in \mathbb{N}$, we consider a uniform partition of the time interval $[0, T]$ with step size $\Delta t := T/L$ and nodes $t_n := n\,\Delta t$, $n = 0, \ldots, L$. The midpoint of each time subinterval is represented as $t_{n+1/2} := \frac{t_{n+1}+t_n}{2}$. For any finite sequence $\{\phi^n,\ n = 0, \ldots, L\}$ of real numbers, we define $\{\phi^n\} := \frac{\phi^{n+1}+\phi^n}{2}$ and introduce the discrete time derivative $\partial_t \phi^n := \frac{\phi^{n+1}-\phi^n}{\Delta t}$. We adopt the same notation for sets of vectors or tensors.

In what follows we utilize the Crank–Nicolson method for the time discretization of (4.3)–(4.4). Namely, for $n = 0, \ldots, L-1$, we seek $\underline{\boldsymbol{\sigma}}_h^{n+1} := (\boldsymbol{\sigma}_{E,h}^{n+1}, \boldsymbol{\sigma}_{V,h}^{n+1}) \in \mathcal{H}_h$ and $\underline{\boldsymbol{u}}_h^{n+1} := (\boldsymbol{u}_h^{n+1}, \hat{\boldsymbol{u}}_h^{n+1}) \in \mathcal{V}_h$ solution of

$$\begin{aligned} &(\partial_t \underline{\boldsymbol{\sigma}}_h^n, \underline{\boldsymbol{\tau}})_{\mathcal{H}} + (\rho \partial_t \boldsymbol{u}_h^n, \boldsymbol{v})_{\mathcal{T}_h} + (\mathcal{G} \left\{ \boldsymbol{\sigma}_{V,h}^n \right\}, \omega \boldsymbol{\tau}_V)_{\mathcal{T}_h} \\ &\quad + B_h(\left\{ \underline{\boldsymbol{\sigma}}_h^n \right\}, \underline{\boldsymbol{v}}) - B_h(\underline{\boldsymbol{\tau}}, \left\{ \underline{\boldsymbol{u}}_h^n \right\}) + \langle \tfrac{(k+1)^2}{h_{\mathcal{F}}} [\![\left\{ \underline{\boldsymbol{u}}_h^n \right\}]\!], [\![\underline{\boldsymbol{v}}]\!] \rangle_{\partial\mathcal{T}_h} = (\left\{ \boldsymbol{f}(t_n) \right\}, \boldsymbol{v})_{\mathcal{T}_h} \end{aligned} \tag{5.1}$$

for all $\underline{\boldsymbol{\tau}} = (\boldsymbol{\tau}_E, \boldsymbol{\tau}_V) \in \mathcal{H}_h$ and $\underline{\boldsymbol{v}} = (\boldsymbol{v}, \hat{\boldsymbol{v}}) \in \mathcal{V}_h$. we assume that the scheme (5.1) is initiated with

$$\underline{\boldsymbol{\sigma}}_h^0 = \underline{\Pi}_{\mathcal{T}}^k(\boldsymbol{\sigma}_E^0, \boldsymbol{\sigma}_V^0), \quad \underline{\boldsymbol{u}}_h^0 = \Xi_{\mathcal{T}}^{k+1} \underline{i}(\boldsymbol{d}^1). \tag{5.2}$$

We point out that at each iteration step of (5.1) we need to solve the square system of linear equations whose matrix is associated to the bilinear form $A_h(\cdot,\cdot) :\ \mathcal{H}_h \times \mathcal{V}_h \to \mathbb{R}$ defined by

$$\begin{aligned} A_h((\underline{\boldsymbol{\sigma}}_h, \underline{\boldsymbol{u}}), (\underline{\boldsymbol{\tau}}_h, \underline{\boldsymbol{v}}_h)) &:= \tfrac{1}{\Delta t}(\underline{\boldsymbol{\sigma}}_h, \underline{\boldsymbol{\tau}}_h)_{\mathcal{H}} + \tfrac{1}{\Delta t}(\rho \boldsymbol{u}_h, \boldsymbol{v}_h)_{\mathcal{T}_h} + \tfrac{1}{2}(\mathcal{G}\boldsymbol{\sigma}_{V,h}, \omega\boldsymbol{\tau}_V)_{\mathcal{T}_h} \\ &\quad + \tfrac{1}{2} B_h(\underline{\boldsymbol{\sigma}}_h, \underline{\boldsymbol{v}}_h) - \tfrac{1}{2} B_h(\underline{\boldsymbol{\tau}}_h, \underline{\boldsymbol{u}}_h) + \tfrac{1}{2} \langle \tfrac{(k+1)^2}{h_{\mathcal{F}}} [\![\underline{\boldsymbol{u}}_h]\!], [\![\underline{\boldsymbol{v}}]\!] \rangle_{\partial\mathcal{T}_h}. \end{aligned}$$

It is straightforward that the null space of this bilinear form is trivial which demonstrates the well-defined nature of the scheme (5.1)–(5.2).

Our objective is to establish the stability of the fully discrete scheme (5.1) by estimating the projected errors $\underline{\boldsymbol{\pi}}_h^n = \underline{\Pi}_{\mathcal{T}}^k \underline{\boldsymbol{\sigma}}(t_n) - \underline{\boldsymbol{\sigma}}_h^n$ and $\underline{\boldsymbol{e}}_h^n = \Xi_{\mathcal{T}}^{k+1} \underline{i}(\boldsymbol{u}(t_n)) - \underline{\boldsymbol{u}}_h^n$ in terms of $\underline{\chi}^n := \underline{\chi}(t_n)$, $\underline{\boldsymbol{q}}^n := \underline{\boldsymbol{q}}(t_n)$ and consistency quantities arising from the time discretization. We recall that, according to our notations, the components of the projected errors $\underline{\boldsymbol{\pi}}_h^n := (\boldsymbol{\pi}_{E,h}^n, \boldsymbol{\pi}_{V,h}^n) \in \mathcal{H}_h$ and $\underline{\boldsymbol{e}}_h^n := (\boldsymbol{e}_h^n, \hat{\boldsymbol{e}}_h^n) \in \mathcal{V}_h$ are given by

$$\begin{aligned} \boldsymbol{\pi}_{E,h}^n &= \Pi_{\mathcal{T}}^k \boldsymbol{\sigma}_E(t_n) - \boldsymbol{\sigma}_{E,h}^n, \quad \boldsymbol{\pi}_{V,h}^n = \Pi_{\mathcal{T}}^k \boldsymbol{\sigma}_V(t_n) - \boldsymbol{\sigma}_{V,h}^n \\ \boldsymbol{e}_h^n &= \Pi_{\mathcal{T}}^{k+1} \boldsymbol{u}(t_n) - \boldsymbol{u}_h^n, \quad \hat{\boldsymbol{e}}_h^n = \Pi_{\mathcal{F}}^{k+1} \hat{\boldsymbol{u}}(t_n) - \hat{\boldsymbol{u}}_h^n, \end{aligned}$$

where $\hat{\boldsymbol{u}} = \boldsymbol{u}|_{\mathcal{F}_h}$. likewise, by definition, it holds that $\underline{\chi}^n = (\chi_E^n, \chi_V^n)$ and $\underline{\boldsymbol{q}}^n = (\boldsymbol{q}^n, \hat{\boldsymbol{q}}^n)$ with

$$\begin{aligned} \chi_E^n &= \boldsymbol{\sigma}_E(t_n) - \Pi_{\mathcal{T}}^k \boldsymbol{\sigma}_E(t_n), \quad \chi_V^n = \boldsymbol{\sigma}_V(t_n) - \Pi_{\mathcal{T}}^k \boldsymbol{\sigma}_V(t_n) \\ \boldsymbol{q}^n &= \boldsymbol{u}(t_n) - \Pi_{\mathcal{T}}^{k+1} \boldsymbol{u}(t_n), \quad \hat{\boldsymbol{q}}^n = \hat{\boldsymbol{u}}(t_n) - \Pi_{\mathcal{F}}^{k+1} \hat{\boldsymbol{u}}(t_n). \end{aligned}$$

We also use the notations $\boldsymbol{\pi}_h^n := \boldsymbol{\pi}_{E,h}^n + \omega \boldsymbol{\pi}_{V,h}^n$ and $\chi^n := \chi_E^n + \omega \chi_V^n$.

Lemma 5.1. *Let*

$$\underline{\boldsymbol{\sigma}} := (\boldsymbol{\sigma}_E, \boldsymbol{\sigma}_V) \in H^1_{[0,T]}(\mathcal{X}^+) \cap C^1_{[0,T]}(\mathcal{H}) \quad \textit{and} \quad \boldsymbol{u} \in C^1_{[0,T]}(L^2(\Omega, \mathbb{R}^d)) \cap C^0_{[0,T]}(H^1_0(\Omega, \mathbb{R}^d))$$

be the solutions of (2.9) and assume that $\boldsymbol{\sigma} = \boldsymbol{\sigma}_E + \omega \boldsymbol{\sigma}_V \in C^0_{[0,T]}(H^s(\mathcal{T}_h, \mathbb{S}) \cap H(\mathbf{div}, \Omega, \mathbb{S}))$*, with* $s > 1/2$*. There exists a constant* $C > 0$ *independent of* h*,* k *and* ω *such that*

$$\begin{aligned} &\max_n \|\underline{\boldsymbol{\pi}}_h^n\|^2_{\mathcal{H}} + \max_n \|\rho^{1/2} \boldsymbol{e}_h^n\|^2_{0,\mathcal{T}_h} + \Delta t \sum_{n=0}^{L-1} \| \tfrac{(k+1)}{h_{\mathcal{F}}^{1/2}} [\![\left\{ \underline{\boldsymbol{e}}_h^n \right\}]\!] \|^2_{0,\partial\mathcal{T}_h} \leq C \Big(\Delta t \sum_{n=0}^{L-1} \|\partial_t \underline{\boldsymbol{\sigma}}(t_n) - \left\{ \dot{\underline{\boldsymbol{\sigma}}}(t_n) \right\}\|^2_{\mathcal{H}} \\ &\quad + \Delta t \sum_{n=0}^{L-1} \|\rho^{1/2}(\partial_t \boldsymbol{u}(t_n) - \left\{ \dot{\boldsymbol{u}}(t_n) \right\})\|^2_{0,\mathcal{T}_h} + \Delta t \sum_{n=0}^{L-1} \| \tfrac{h_{\mathcal{F}}^{1/2}}{k+1} \{\chi^n\} \boldsymbol{n} \|^2_{0,\partial\mathcal{T}_h} + \Delta t \sum_{n=0}^{L-1} \| \left\{ \underline{\boldsymbol{q}}^n \right\} \|^2_{\mathcal{V}} \Big). \end{aligned} \tag{5.3}$$

Proof. It follows from the consistency Eq. (4.7) and the orthogonality properties employed in the proof of Lemma 4.1 that the projected errors $\underline{\boldsymbol{\pi}}_h^n \in \mathcal{H}_h$ and $\underline{\boldsymbol{e}}_h^n \in \mathcal{V}_h$ satisfy the equation

$$
\begin{aligned}
&(\partial_t \underline{\boldsymbol{\pi}}_h^n, \underline{\boldsymbol{\tau}})_{\mathcal{H}} + (\rho \partial_t \boldsymbol{e}_h^n, \boldsymbol{v})_{\mathcal{T}_h} + (\mathcal{G}\left\{\boldsymbol{\pi}_{V,h}^n\right\}, \omega \boldsymbol{\tau}_V)_{\mathcal{T}_h} + B_h(\left\{\underline{\boldsymbol{\pi}}_h^n\right\}, \underline{\boldsymbol{v}}) - B_h(\underline{\boldsymbol{\tau}}, \left\{\underline{\boldsymbol{e}}_h^n\right\}) \\
&\quad + \langle \tfrac{(k+1)^2}{h_F} [\![\left\{\underline{\boldsymbol{e}}_h^n\right\}]\!], [\![\underline{\boldsymbol{v}}]\!] \rangle_{\partial \mathcal{T}_h} = (\partial_t \underline{\boldsymbol{\sigma}}(t_n) - \left\{\dot{\underline{\boldsymbol{\sigma}}}(t_n)\right\}, \underline{\boldsymbol{\tau}})_{\mathcal{H}} + (\rho(\partial_t \boldsymbol{u}(t_n) - \left\{\dot{\boldsymbol{u}}(t_n)\right\}), \boldsymbol{v})_{\mathcal{T}_h} \\
&\qquad + \langle \{\boldsymbol{\chi}^n\} \boldsymbol{n}, [\![\underline{\boldsymbol{v}}]\!] \rangle_{\partial \mathcal{T}_h} + B_h(\underline{\boldsymbol{\tau}}, \left\{\underline{\boldsymbol{q}}^n\right\}) - \langle \tfrac{(k+1)^2}{h_F} [\![\left\{\underline{\boldsymbol{q}}^n\right\}]\!], [\![\underline{\boldsymbol{v}}]\!] \rangle_{\partial \mathcal{T}_h}
\end{aligned}
\tag{5.4}
$$

for all $\underline{\boldsymbol{\tau}} = (\boldsymbol{\tau}_E, \boldsymbol{\tau}_V) \in \mathcal{H}_h$ and $\underline{\boldsymbol{v}} = (\boldsymbol{v}, \hat{\boldsymbol{v}}) \in \mathcal{V}_h$. Selecting $\underline{\boldsymbol{\tau}} = \left\{\underline{\boldsymbol{\pi}}_h^n\right\}$ and $\underline{\boldsymbol{v}} = \left\{\underline{\boldsymbol{e}}_h^n\right\}$ in Eq. (5.4), taking into account that the bilinear form associated with the tensor $\mathcal{G}$ is non-negative and applying (4.2) and the Cauchy–Schwartz inequality to the terms on the right-hand side we derive the estimate

$$
\begin{aligned}
&\frac{1}{2\Delta t}\left(\|\underline{\boldsymbol{\pi}}_h^{n+1}\|_{\mathcal{H}}^2 + \|\rho^{1/2} \boldsymbol{e}_h^{n+1}\|_{0,\mathcal{T}_h}^2 - \|\underline{\boldsymbol{\pi}}_h^n\|_{\mathcal{H}}^2 - \|\rho^{1/2} \boldsymbol{e}_h^n\|_{0,\mathcal{T}_h}^2 \right) + \| \tfrac{k+1}{h_F^{1/2}} [\![\left\{\underline{\boldsymbol{e}}_h^n\right\}]\!] \|_{0,\partial \mathcal{T}_h}^2 \\
&\le \|\partial_t \underline{\boldsymbol{\sigma}}(t_n) - \left\{\dot{\underline{\boldsymbol{\sigma}}}(t_n)\right\}\|_{\mathcal{H}} \|\left\{\underline{\boldsymbol{\pi}}_h^n\right\}\|_{\mathcal{H}} + \|\rho^{1/2}(\partial_t \boldsymbol{u}(t_n) - \left\{\dot{\boldsymbol{u}}(t_n)\right\})\|_{0,\mathcal{T}_h} \|\rho^{1/2} \left\{\boldsymbol{e}_h^n\right\}\|_{0,\mathcal{T}_h} \\
&+ \| \tfrac{h_F^{1/2}}{k+1} \{\boldsymbol{\chi}^n\} \boldsymbol{n} \|_{0,\partial \mathcal{T}_h} \| \tfrac{k+1}{h_F^{1/2}} [\![\left\{\underline{\boldsymbol{e}}_h^n\right\}]\!] \|_{0,\partial \mathcal{T}_h} + \|\left\{\underline{\boldsymbol{\pi}}_h^n\right\}\|_{\mathcal{H}} \| \left\{\underline{\boldsymbol{q}}^n\right\} \|_{\mathcal{V}} + \| \tfrac{k+1}{h_F^{1/2}} [\![\left\{\underline{\boldsymbol{q}}^n\right\}]\!] \|_{0,\partial \mathcal{T}_h} \| \tfrac{k+1}{h_F^{1/2}} [\![\left\{\underline{\boldsymbol{e}}_h^n\right\}]\!] \|_{0,\partial \mathcal{T}_h}.
\end{aligned}
$$

Next, employing a standard summation procedure and taking into account that the projected errors vanish identically at the initial step we get

$$
\begin{aligned}
&\max_n \|\underline{\boldsymbol{\pi}}_h^n\|_{\mathcal{H}}^2 + \max_n \|\rho^{1/2} \boldsymbol{e}_h^n\|_{0,\mathcal{T}_h}^2 + \Delta t \sum_{n=0}^{L-1} \| \tfrac{(k+1)}{h_F^{1/2}} [\![\left\{\underline{\boldsymbol{e}}_h^n\right\}]\!] \|_{0,\partial \mathcal{T}_h}^2 \\
&\quad \lesssim \max_n \|\underline{\boldsymbol{\pi}}_h^n\|_{\mathcal{H}} \Big(\Delta t \sum_{n=0}^{L-1} \|\partial_t \underline{\boldsymbol{\sigma}}(t_n) - \left\{\dot{\underline{\boldsymbol{\sigma}}}(t_n)\right\}\|_{\mathcal{H}} \Big) \\
&\quad + \max_n \|\rho^{1/2} \boldsymbol{e}_h^n\|_{0,\mathcal{T}_h} \Big(\Delta t \sum_{n=0}^{L-1} \|\rho^{1/2}(\partial_t \boldsymbol{u}(t_n) - \left\{\dot{\boldsymbol{u}}(t_n)\right\})\|_{0,\mathcal{T}_h} \Big) \\
&\quad + \Delta t \sum_{n=0}^{L-1} \| \tfrac{h_F^{1/2}}{k+1} \{\boldsymbol{\chi}^n\} \boldsymbol{n} \|_{0,\partial \mathcal{T}_h} \| \tfrac{k+1}{h_F^{1/2}} [\![\left\{\underline{\boldsymbol{e}}_h^n\right\}]\!] \|_{0,\partial \mathcal{T}_h} + \max_n \|\underline{\boldsymbol{\pi}}_h^n\|_{\mathcal{H}} \Big(\Delta t \sum_{n=0}^{L-1} \| \left\{\underline{\boldsymbol{q}}^n\right\} \|_{\mathcal{V}} \Big) \\
&\quad + \Delta t \sum_{n=0}^{L-1} \| \tfrac{k+1}{h_F^{1/2}} [\![\left\{\underline{\boldsymbol{q}}^n\right\}]\!] \|_{0,\partial \mathcal{T}_h} \| \tfrac{k+1}{h_F^{1/2}} [\![\left\{\underline{\boldsymbol{e}}_h^n\right\}]\!] \|_{0,\partial \mathcal{T}_h}.
\end{aligned}
$$

Finally, applying repeatedly Young's inequality $2ab \le \frac{a^2}{\epsilon} + \epsilon b^2$, with a suitable $\epsilon > 0$ in each instance, and subsequently applying the Cauchy–Schwartz inequality for the summation terms, we obtain (5.3). □

Performing a Taylor expansion centered at $t = t_{n+1/2}$ we obtain the identity

$$
\partial_t \varphi(t_n) - \left\{\dot{\varphi}(t_n)\right\} = \frac{(\Delta t)^2}{16} \int_{-1}^{1} \ddot{\varphi}(t_{n+1/2} + \tfrac{\Delta t}{2} s)(|s|^2 - 1)\, \mathrm{d}s \quad \forall \varphi \in C^3([0,T]), \quad 0 \le n \le L-1.
$$

Hence, if we add to the regularity assumptions imposed in Lemma 5.1 to the exact the solutions of (2.9) the time regularity assumptions $\underline{\boldsymbol{\sigma}} \in C^3_{[0,T]}(\mathcal{H})$ and $\boldsymbol{u} \in C^3_{[0,T]}(L^2(\Omega, \mathbb{R}^d))$, we deduce from (5.3) that

$$
\begin{aligned}
&\max_n \|\underline{\boldsymbol{\pi}}_h^n\|_{\mathcal{H}} + \max_n \|\rho^{1/2} \boldsymbol{e}_h^n\|_{0,\mathcal{T}_h} + \Big(\Delta t \sum_{n=0}^{L-1} \| \tfrac{(k+1)}{h_F^{1/2}} [\![\left\{\underline{\boldsymbol{e}}_h^n\right\}]\!] \|_{0,\partial \mathcal{T}_h}^2 \Big)^{1/2} \\
&\quad \lesssim (\Delta t)^2 \big(\max_{[0,T]} \|\ddot{\underline{\boldsymbol{\sigma}}}\|_{\mathcal{H}} + \max_{[0,T]} \|\ddot{\boldsymbol{u}}\|_{0,\mathcal{T}_h} \big) + \max_n \| \tfrac{h_F^{1/2}}{k+1} \boldsymbol{\chi}^n \boldsymbol{n} \|_{0,\partial \mathcal{T}_h}^2 + \max_n \|\underline{\boldsymbol{q}}^n\|_{\mathcal{V}}.
\end{aligned}
\tag{5.5}
$$

Theorem 5.1. *Assume that the solution $(\underline{\boldsymbol{\sigma}}, \underline{\boldsymbol{u}})$ of (2.9) satisfies the time regularity assumptions $\underline{\boldsymbol{\sigma}} := (\boldsymbol{\sigma}_E, \boldsymbol{\sigma}_V) \in H^1_{[0,T]}(\mathcal{X}^+) \cap C^3_{[0,T]}(\mathcal{H})$, $\boldsymbol{u} \in C^3_{[0,T]}(L^2(\Omega, \mathbb{R}^d)) \cap C^0_{[0,T]}(H^1_0(\Omega, \mathbb{R}^d))$ and the piecewise space regularity conditions $\boldsymbol{\sigma}_E, \boldsymbol{\sigma}_V \in C^0(H^{1+r}(\cup_j \Omega_j, \mathbb{S}))$ and $\boldsymbol{u} \in C^0(H^{2+r}(\cup_j \Omega_j, \mathbb{R}^d))$, with $r \ge 0$. Then, there exists a constant $C > 0$ independent of h, k, and ω such that*

$$
\begin{aligned}
&\max_n \|\underline{\boldsymbol{\sigma}}(t_n) - \underline{\boldsymbol{\sigma}}_h^n\|_{\mathcal{H}} + \max_n \|\boldsymbol{u}(t_n) - \boldsymbol{u}_h^n\|_{0,\mathcal{T}_h} + \left(\Delta t \sum_{n=0}^{L-1} \| \tfrac{k+1}{h_F^{1/2}} [\![\underline{i}(\boldsymbol{u}(t_n)) - \underline{\boldsymbol{u}}_h^n]\!] \|_{0,\partial \mathcal{T}_h}^2 \, dt \right)^{1/2} \\
&\le C \tfrac{h_K^{\min\{r,k\}+1}}{(k+1)^{r+1}} \Big(\sum_{j=1}^{J} (\max_{[0,T]} \|\boldsymbol{\tau}_E\|_{1+r,\Omega_j}^2 + \omega_j^2 \max_{[0,T]} \|\boldsymbol{\tau}_V\|_{1+r,\Omega_j}^2 + \max_{[0,T]} \|\boldsymbol{u}\|_{2+r,\Omega_j}^2) \Big)^{1/2} \\
&\quad + C(\Delta t)^2 \big(\max_{[0,T]} \|\ddot{\underline{\boldsymbol{\sigma}}}\|_{\mathcal{H}} + \max_{[0,T]} \|\ddot{\boldsymbol{u}}\|_{0,\mathcal{T}_h} \big) \quad \forall k \ge 0.
\end{aligned}
$$

Table 6.1
Error progression is shown for a sequence of uniform refinements in space and over-refinements in time. The errors are measured at $T = 1.5$, with $\rho = \omega = 1$ and by employing the Lamé coefficients defined in Eq. (6.3). The exact solution is provided by Eq. (6.1) by imposing pure Dirichlet boundary condition.

k	h	$\mathrm{e}_{hk}^L(\boldsymbol{\sigma})$	$\mathrm{r}_{hk}^L(\boldsymbol{\sigma})$	$\mathrm{e}_{hk}^L(\boldsymbol{u})$	$\mathrm{r}_{hk}^L(\boldsymbol{u})$
0	1/4	1.65e+00	*	3.54e−01	*
	1/8	7.91e−01	1.06	8.78e−02	2.01
	1/16	3.64e−01	1.12	2.14e−02	2.04
	1/32	1.81e−01	1.01	5.56e−03	1.94
1	1/4	6.42e−02	*	4.18e−03	*
	1/8	1.47e−02	2.13	4.96e−04	3.07
	1/16	3.31e−03	2.15	5.43e−05	3.19
	1/32	8.20e−04	2.01	7.48e−06	2.86
2	1/2	2.98e−02	*	2.25e−03	*
	1/4	1.64e−03	4.18	5.38e−05	5.39
	1/8	1.78e−04	3.21	2.79e−06	4.27
	1/16	1.91e−05	3.22	1.42e−07	4.30
3	1/2	1.15e−03	*	6.20e−05	*
	1/4	2.55e−05	5.50	6.26e−07	6.63
	1/8	1.35e−06	4.24	1.50e−08	5.38

Proof. Applying the triangle inequality in (5.5) we deduce that

$$\max_n \|\underline{\boldsymbol{\sigma}}(t_n) - \underline{\boldsymbol{\sigma}}_h^n\|_{\mathcal{H}} + \max_n \|\boldsymbol{u}(t_n) - \boldsymbol{u}_h^n\|_{0,\mathcal{T}_h} + \left(\Delta t \sum_{n=0}^{L-1} \| \tfrac{k+1}{h_F^{1/2}} [\![\underline{i}(\boldsymbol{u}(t_n)) - \underline{\boldsymbol{u}}_h^n]\!] \|_{0,\partial\mathcal{T}_h}^2 \, \mathrm{d}t \right)^{1/2}$$
$$\lesssim \max_n \|\underline{\boldsymbol{\chi}}^n\|_{\mathcal{H}} + \max_n \| \tfrac{h_F^{1/2}}{k+1} \boldsymbol{\chi}^n \boldsymbol{n} \|_{0,\partial\mathcal{T}_h}^2 + \max_n \|\underline{\boldsymbol{q}}^n\|_{\mathcal{V}} + C(\Delta t)^2 \big(\max_{[0,T]} \|\ddot{\underline{\boldsymbol{\sigma}}}\|_{\mathcal{H}} + \max_{[0,T]} \|\ddot{\boldsymbol{u}}\|_{0,\mathcal{T}_h} \big)$$

and the result is a direct consequence of the error estimates (3.8) and (3.10). □

6. Numerical results

The numerical results presented in this section have been implemented using the finite element library `Netgen/NGSolve` [38].

Accuracy verification

To confirm the decay of error as predicted by Theorem 5.1 with respect to the parameters h, Δt and k, we compare the computed solutions at different levels of refinement to a closed-form exact solution of problem (2.9) obtained from a displacement field given by

$$\boldsymbol{d}(x, y, t) := \begin{pmatrix} \cos(t)\sin(x)e^{-y} \\ e^{t+x}\cos(y) \end{pmatrix} \quad \text{in } \Omega \times [0, T], \tag{6.1}$$

where $\Omega = (0, 1)^2$. We assume that the medium characterized by (2.1) is isotropic in the sense that the fourth-order elastic and viscoelastic tensors are defined by

$$C\boldsymbol{\tau} = 2\mu_C \boldsymbol{\zeta} + \lambda_C \operatorname{tr}(\boldsymbol{\zeta}) I \qquad \mathcal{D}\boldsymbol{\zeta} = 2\mu_D \boldsymbol{\tau} + \lambda_D \operatorname{tr}(\boldsymbol{\zeta}) I, \tag{6.2}$$

in terms of Lamé coefficients $\mu_C > 0$, $\lambda_C > 0$, $\mu_D > 0$, and $\lambda_D > 0$. The exact displacement (6.1) is used to construct exact elastic and viscous stresses as well as appropriate initial conditions (5.2) and non-homogeneous boundary conditions.

The time interval $[0, T]$ is equally divided into sub-intervals of length Δt. Since the error from the Crank–Nicolson method is $O(\Delta t^2)$, we choose $\Delta t \simeq O(h^{(k+2)/2})$ so that the error from the time discretization does not pollute the order of convergence of the space discretization. For tables and figures presenting accuracy verification, we use the following notation for the L^2-norms of the errors:

$$\mathrm{e}_{hk}^L(\boldsymbol{\sigma}) := \|\underline{\boldsymbol{\sigma}}(T) - \underline{\boldsymbol{\sigma}}_h^L\|_{\mathcal{H}}, \qquad \mathrm{e}_{hk}^L(\boldsymbol{u}) := \|\boldsymbol{u}(T) - \boldsymbol{u}_h^L\|_{0,\Omega}.$$

The rates of convergence in space are computed as

$$\mathrm{r}_{hk}^L(\star) = \log(\mathrm{e}_{hk}^L(\star)/\tilde{\mathrm{e}}_{hk}^L(\star))[\log(h/\tilde{h})]^{-1} \quad \star \in \{\boldsymbol{\sigma}, \boldsymbol{u}\},$$

where $\mathrm{e}_{hk}^L(\star)$, $\tilde{\mathrm{e}}_{hk}^L(\star)$ denote errors generated on two consecutive meshes of sizes h and $\tilde{h}$, respectively.

In our first test we apply a pure Dirichlet boundary condition, which results in an empty set for Γ_N while Γ_D corresponds to the entire boundary Γ. The Lamé coefficients are chosen as

$$\mu_C = 1, \quad \lambda_C = 3, \quad \mu_D = 2, \quad \text{and} \quad \lambda_D = 4. \tag{6.3}$$

Table 6.2
Error progression is shown for a sequence of uniform refinements in space and over-refinements in time. The errors are measured at $T = 1.5$, with $\rho = \omega = 1$ and by employing the Lamé coefficients resulting from (6.4). The exact solution is provided by Eq. (6.1) by imposing a Dirichlet-Neumann boundary condition.

k	h	$\mathrm{e}^L_{hk}(\boldsymbol{\sigma})$	$\mathrm{r}^L_{hk}(\boldsymbol{\sigma})$	$\mathrm{e}^L_{hk}(\boldsymbol{u})$	$\mathrm{r}^L_{hk}(\boldsymbol{u})$
0	1/8	8.93e+03	*	1.36e+04	*
	1/16	4.80e+03	0.90	3.07e+03	2.14
	1/32	2.38e+03	1.01	7.55e+02	2.03
	1/64	1.00e+03	1.25	1.85e+02	2.03
1	1/4	1.21e+03	*	6.77e+02	*
	1/8	2.08e+02	2.54	7.50e+01	3.17
	1/16	5.26e+01	1.98	7.75e+00	3.28
	1/32	1.24e+01	2.09	9.59e−01	3.01
2	1/4	2.28e+01	*	8.82e+00	*
	1/8	2.17e+00	3.39	4.69e−01	4.23
	1/16	2.45e−01	3.14	2.25e−02	4.38
	1/32	2.97e−02	3.05	1.39e−03	4.01
3	1/4	3.79e−01	*	9.82e−02	*
	1/8	1.91e−02	4.31	2.45e−03	5.33
	1/16	8.92e−04	4.42	5.44e−05	5.49

Table 6.3
Computed errors for a sequence of uniform refinements in time with $h = 1/16$ and $k = 4$. The errors are measured at $t = T = 1$, with $\rho = \omega = 1$ and by employing the Lamé coefficients defined in Eq. (6.3). The exact solution is provided by Eq. (6.1) by imposing pure Dirichlet boundary condition.

Δt	$\mathrm{e}^L_{hk}(\boldsymbol{\sigma})$	$\mathrm{r}^L_{hk}(\boldsymbol{\sigma})$	$\mathrm{e}^L_{hk}(\boldsymbol{u})$	$\mathrm{r}^L_{hk}(\boldsymbol{u})$
1/32	3.24×10^{-4}	*	1.72×10^{-5}	*
1/64	8.30×10^{-5}	+1.96	4.78×10^{-6}	+1.85
1/128	2.10×10^{-5}	+1.98	1.25×10^{-6}	+1.94
1/256	5.28×10^{-6}	+1.99	3.17×10^{-7}	+1.97
1/512	1.32×10^{-6}	+2.00	8.00×10^{-8}	+1.99

Additionally, we set $\omega = 1$ and $\rho = 1$ for the remaining parameters. Table 6.1 displays the errors with respect to the mesh size h for four different polynomial degrees k. We observe that the convergence in the stress field attains the optimal rate of $O(h^{k+1})$. Furthermore, as mentioned earlier in Remark 4.1, the velocity demonstrates a convergence rate of $O(h^{k+2})$, which is one order superior to what is stated in Theorem 5.1.

To verify the accuracy and stability of the scheme in the nearly incompressible limit we repeat the same experiment and consider this time material parameter sets (Young's modulus and Poisson ratio)

$$E_C = 0.49, \quad \nu_C = 100, \quad E_D = 0.4999, \quad \nu_D = 1000, \tag{6.4}$$

which give Lamé constants $\lambda_\star = \frac{E_\star \nu_\star}{(1+\nu_\star)(1-2\nu_\star)}$ and $\mu_\star = \frac{E_\star}{2(1+\nu_\star)}$, $\star \in \{C, D\}$. We recall that the dissipativity condition requires that $\mu_D > \mu_C$ and $\lambda_D > \lambda_C$. We also impose in this second test a Dirichlet boundary condition on the bottom side $\Gamma_D = (0,1) \times \{0\}$ and a Neumann boundary condition on the remaining three sides of the unit square. The error decay for this case is collected in Table 6.2. These results demonstrate the ability of the proposed HDG scheme to produce accurate approximations also in the nearly incompressible viscoelasticity regime.

On the other hand, Table 6.3 portrays the convergence results obtained after fixing the mesh size to $h = 1/16$ and the polynomial degree to $k = 4$ and varying the time step Δt discretizing the time interval $[0, T]$, with $T = 1$. The rates of convergence in time, are computed as

$$\mathrm{r}^L_{hk}(\star) = \log(\mathrm{e}^L_{hk}(\star)/\tilde{\mathrm{e}}^L_{hk}(\star))[\log(\Delta t/\widetilde{\Delta t})]^{-1} \quad \star \in \{\boldsymbol{\sigma}, \boldsymbol{u}\},$$

where e^L_{hk}, $\tilde{\mathrm{e}}^L_{hk}$ denote errors generated on two consecutive runs considering time steps Δt and $\widetilde{\Delta t}$, respectively. In this example, we consider the same manufactured solution obtained from (6.1) with $\Gamma_D = \Gamma$. The remaining parameters are given by $\omega = 1$, $\rho = 1$, and (6.3). The expected convergence rate of $O([\Delta t]^2)$ is attained as the time step is refined.

Finally, we fix the space mesh size $h = 0.25$ and the time mesh size $\Delta t = 10^{-6}$ and let k vary from 0 to 5. In Fig. 6.1 we report the error $\mathrm{e}^L_{hk}(\boldsymbol{\sigma})$ in the stress variable and the error $\mathrm{e}^L_{hk}(\boldsymbol{u})$ in velocity at $T = 0.5$ as a function of the polynomial degree $k + 1$ in a semi-logarithmic scale. As expected, an exponential convergence is observed.

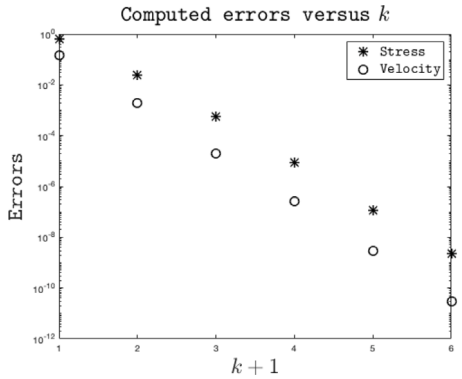

Fig. 6.1. Computed errors versus the polynomial degree k with $h = 1/4$ and $\Delta t = 10^{-6}$. The errors are measured at $t = T = 0.5$, with $\rho = \omega = 1$ and by employing the Lamé coefficients defined in Eq. (6.3). The exact solution is provided by Eq. (6.1) by imposing pure Dirichlet boundary condition.

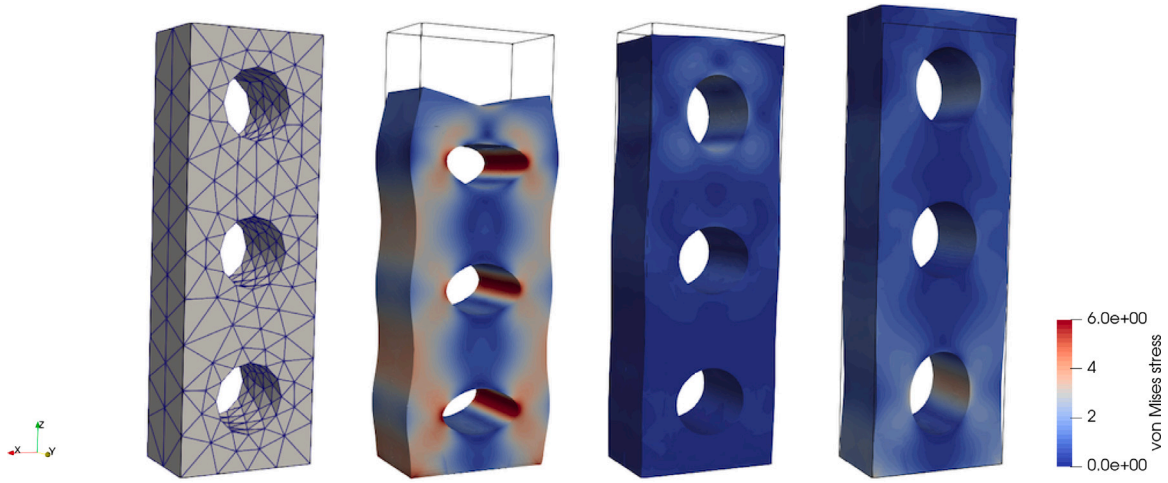

Fig. 6.2. On the left, we present the meshed domain, while the next three figures depict snapshots of the viscoelastic body's deformed configurations at times 2 s, 3.5 s, and 4.5 s, respectively. The color map in each figure indicates the distribution of von Mises stresses. The results are obtained by employing the boundary conditions (6.5) and the viscoelastic material parameters defined in (6.6), and by setting $h = 0.3$, $k = 3$, and $\Delta t = 0.05$. (For interpretation of the references to color in this figure legend, the reader is referred to the web version of this article.)

Comparative of mechanical behavior in 3D: elastodynamic and dynamic/quasi-static viscoelasticity testing of a perforated brick

We use our HDG method to solve a three-dimensional model problem where an exact solution is unavailable. The objective is to simulate the transient behavior of a viscoelastic perforated brick under dynamic and quasi-static conditions, including purely elastic behavior.

The computational domain Ω is a rectangular cuboid with dimensions $(0,1)\times(0,0.6)\times(0,3)\,\mathrm{m}^3$ containing three right circular cylindrical holes centered at $(0.5,0,0.5)$, $(0.5,0,1.5)$, and $(0.5,0,2.5)$. These cylindrical holes are oriented parallel to the y-direction and have radii of 0.25 and heights of 0.6. We refer to Fig. 6.2 for a visual representation of this geometry.

We assume that the solid represented by Ω has mass density of $\rho = 1\,\mathrm{kg/m}^3$. At $t = 0.5$ s, an instantaneous traction of 1 Pa is applied in the negative z direction on the upper face Γ_N^1, which lies in the plane $z = 1$. This traction is maintained for a duration of 2.5 s, after which it is abruptly released. The boundary face Γ_D at $z = 0$ is clamped, while the remaining boundary $\Gamma_N^2 := \partial\Omega\backslash\Gamma_D\cup\Gamma_N^1$ is left stress-free. Summing up, we are imposing to problem (2.4) vanishing initial data with the following loading and boundary conditions:

$$\begin{aligned} &\boldsymbol{f} = \mathbf{0} \text{ in } \Omega\times(0,T], \quad \boldsymbol{d} = \mathbf{0} \text{ on } \Gamma_D\times(0,T],\\ &\boldsymbol{\sigma n} = \begin{cases} -1 & \text{if } 0.5 \le t \le 3\\ 0 & \text{otherwise} \end{cases} \text{ on } \Gamma_N^1\times(0,T], \quad \boldsymbol{\sigma n} = \mathbf{0} \text{ on } \Gamma_N^2\times(0,T]. \end{aligned} \tag{6.5}$$

We consider again tensors $\mathcal{C}$ and $\mathcal{D}$ given by (6.2) with material parameters

$$\lambda_C = 6\,\mathrm{Pa}, \quad \mu_C = 9\,\mathrm{Pa}, \quad \lambda_D = 9\,\mathrm{Pa}, \quad \mu_D = 15\,\mathrm{Pa}, \quad \omega = 0.7\,\mathrm{s}. \tag{6.6}$$

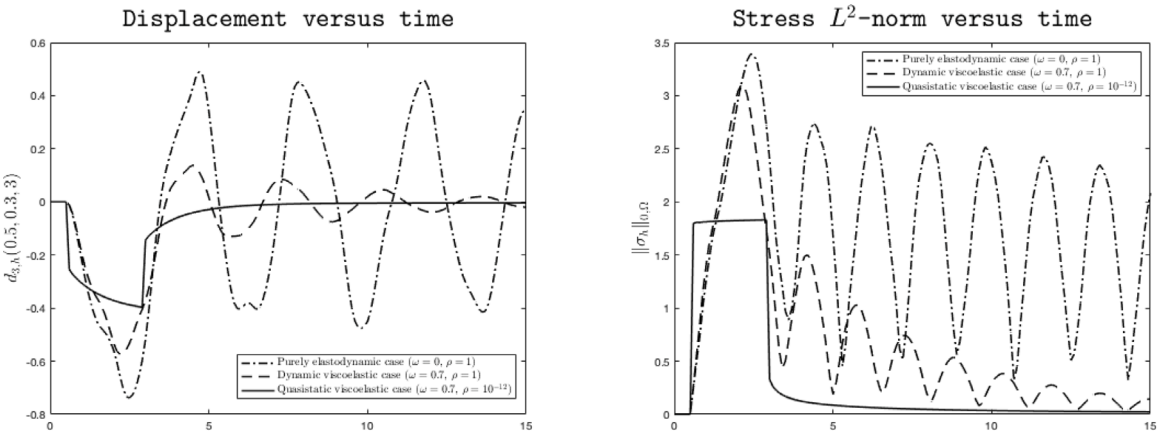

Fig. 6.3. The transients of the z-component of displacement at coordinates (0.5, 0.3, 3.0) are shown on the left, while the L^2-norm of the global stress tensor is displayed on the right. The results are presented for three cases: purely elastodynamic (represented by a line with the marker ·—), dynamic viscoelastic (represented by a dashed line), and quasi-static viscoelastic (represented by a continuous line). These results are obtained using the boundary conditions (6.5), the Lamé coefficients provided in (6.6), and setting $h = 0.2$, $k = 1$, and $\Delta t = 0.1$. The values of ρ and ω corresponding to each case are indicated in the figure.

We obtain an approximate solution of the problem by using the numerical method (5.1) with a polynomial degree $k = 3$, a mesh size $h = 0.3$ and a time step of $\Delta t = 0.05$ s. In Fig. 6.2, we illustrate the meshed domain and we show three snapshots (at times 2 s, 3.5 s, and 4.5 s) representing the von Mises stresses portrayed on the deformed domain. For this purpose, the approximate displacements are post-processed from the velocity field using the formula

$$\boldsymbol{d}_h^{n+1} = \boldsymbol{d}_h^n + \Delta t\ (\boldsymbol{u}_h^{n+1} + \boldsymbol{u}_h^n)/2.$$

In Fig. 6.3, we present a comparison between the results obtained using Zener's model for dynamic and quasi-static viscoelasticity, and also the results obtained in the purely elastodynamic case. To simulate the standard viscoelastic model without inertia, we impose a small mass density ρ (specifically, in the results depicted in Fig. 6.3, we set $\rho = 10^{-12}\,\mathrm{kg/m^3}$) while keeping the other parameters unchanged. The purely elastic scenario is achieved by setting $\omega = 0$ across the entire domain. In all three cases, we conducted the tests until $t = 15$ s with $k = 1$, $h = 0.2$ and $\Delta t = 0.1$. We depict the evolution of the third components of the approximate displacement fields at (0.5, 0.3, 3) on the left panel, and the L^2-norms of the approximate stress tensors on the right panel in Fig. 6.3.

The displacement profile observed under quasi-static conditions exhibits the expected behavior associated with creep phenomena, as described in previous works such as [6, Section 6.2.2 and Figure 6] and [10, Figure 6.3], which employed 2D and 3D numerical tests for stress formulations of Zener's viscoelastic model. Additionally, the dynamic viscoelastic case demonstrates a clear dissipative character when compared to the elastodynamic case. The same conclusion applies to the plots displaying the L^2-norms of the stress tensors.

Wave propagation in a composite material

In order to test the capability of our approach in considering composite materials with mixed viscoelastic properties we employ an illustrative example inspired by [5, Section 5.2.2]. However, while the reference focuses on simulating wave propagation in distinct domains featuring either elastic or viscoelastic properties, our experiment explores the dynamics of an elastic wave within a hybrid medium combining both viscoelastic and purely elastic regions.

We consider a domain $\Omega = (-8, 8)^2$ representing a solid with viscoelastic properties in $\Omega_V = (-8, 0) \times (-8, 8)$ and purely elastic behavior in $\Omega_E = (0, 8) \times (-8, 8)$. The physical parameters considered in each medium are indicated in Fig. 6.4. We take the initial data equal to 0 and impose an homogeneous Dirichlet boundary condition on Γ.

We consider a compactly supported volume force $\boldsymbol{f}(x, y, t) := \boldsymbol{g}(x, y)p(t)$, where

$$\boldsymbol{g}(x,y) = \begin{cases} (1 - 4\|\boldsymbol{r}\|^2)\frac{\boldsymbol{r}}{\|\boldsymbol{r}\|} & \text{if } \|\boldsymbol{r}\| < 1/2 \\ 0 & \text{otherwise} \end{cases} \quad \text{and} \quad p(t) := \begin{cases} \frac{\mathrm{d}}{\mathrm{d}t}[e^{-(15\pi)^2(t-\frac{1}{15})^2}] & \text{if } t < \frac{2}{15} \\ 0 & \text{otherwise} \end{cases}$$

with $\boldsymbol{r} := (x, y)^{\mathrm{t}}$. Graphic representations of the vector field $\boldsymbol{g}$ and the function p are given in Fig. 6.4.

We numerically solve problem (5.1) using the data described earlier, employing a mesh size of $h = 0.1$, a time step of $\Delta t = 0.01$, and a polynomial degree of $k = 2$. Fig. 6.5 illustrates the magnitude of the displacement field obtained at various time intervals: 0.5 s, 1 s, 1.5 s, and 2 s. Notably, we observe distinct behaviors in the wave propagation within the composite medium. Specifically, the wave propagates at a faster rate and experiences more significant damping in the viscoelastic region.

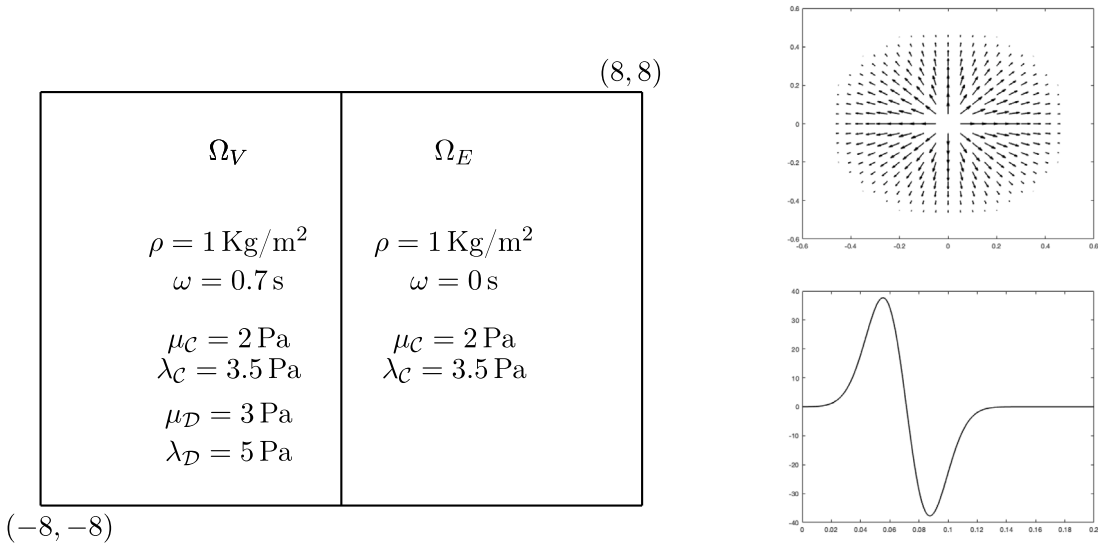

Fig. 6.4. The partition of the computational domain Ω into a part Ω_E with purely elastic behavior and a Ω_V with viscoelastic properties (left). We indicate the Lamé coefficients, the mass density and the relaxation time corresponding to each region. Graphical representations of the vector field $\boldsymbol{g}$ and the scalar function p defining the body force by $\boldsymbol{f} = p(t)\boldsymbol{g}(x, y)$ (right).

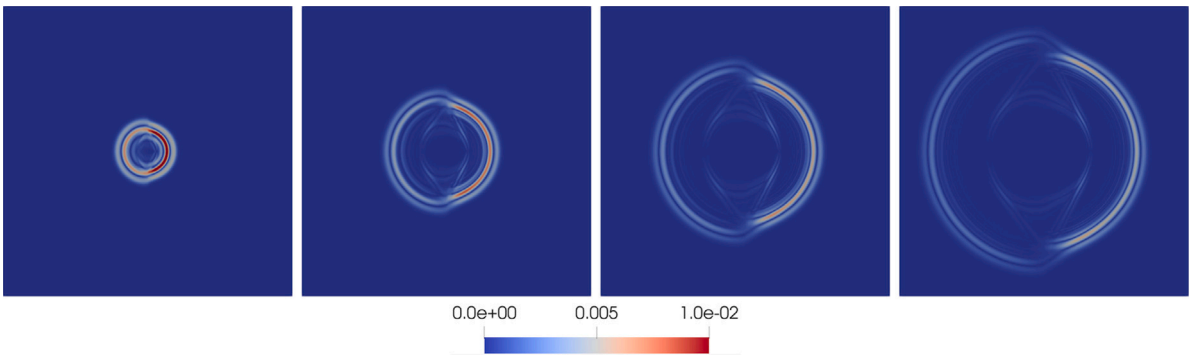

Fig. 6.5. Snapshots of the displacement magnitude at times 0.5 s, 1 s, 1.5 s, 2 s. The results are obtained with vanishing initial data, utilizing the coefficients provided in Fig. 6.4 and the source term $\boldsymbol{f} = p(t)\boldsymbol{g}(x, y)$. Homogeneous Dirichlet boundary conditions were applied, and the numerical parameters were set as follows: $h = 0.1$, $k = 2$, and $\Delta t = 0.01$.

7. Conclusion

We have introduced a parameter-free hybrid discontinuous Galerkin (HDG) method for the stress-velocity formulation of Zener's viscoelasticity model. Taking advantage of the inherent hybridization strategy of the HDG framework, the method enables a substantial reduction in globally coupled degrees of freedom, thereby enhancing computational efficiency without compromising accuracy. The method employs symmetric tensor-valued piecewise polynomials of arbitrary degree to provide accurate stress approximations in both two- and three-dimensional domains. Moreover, the method's versatility extends to heterogeneous materials with composite elastic-viscoelastic components.

We have presented an *hp*-finite element analysis that establishes the stability of the proposed HDG semi-discrete scheme with respect to the discretization parameters h and k, as well as the characteristic relaxation time ω. We have derived error estimates proving quasi-optimal convergence of the stress variable in terms of mesh size, alongside suboptimal convergence of the velocity. Furthermore, we have applied the Crank–Nicolson rule as a time-stepping scheme to the proposed HDG method, and shown the stability of the resulting fully-discrete scheme and analyzed its convergence properties. The numerical results corroborate our theoretical predictions.

Declaration of competing interest

The authors declare that they have no known competing financial interests or personal relationships that could have appeared to influence the work reported in this paper.

Data availability

Data will be made available on request.

References

[1] C. Zener, Elasticity and Anelasticity of Metals, Univ. of Chicago Press, Chicago, 1948.
[2] J. Salençon, Viscoelastic Modeling for Structural Analysis, John Wiley & Sons, 2019.
[3] M. Fabrizio, A. Morro, Mathematical Problems in Linear Viscoelasticity, SIAM, Philadelphia, 1992.
[4] S. Shaw, J.R. Whiteman, Numerical solution of linear quasistatic hereditary viscoelasticity problems, SIAM J. Numer. Anal. 38 (2000) 80–97.
[5] E. Bécache, A. Ezziani, P. Joly, A mixed finite element approach for viscoelastic wave propagation, Comput. Geosci. 8 (2005) 255–299.
[6] M. Rognes, R. Winther, Mixed finite element methods for linear viscoelasticity using weak symmetry, Math. Models Methods Appl. Sci. 20 (2010) 955–985.
[7] J.J. Lee, Analysis of mixed finite element methods for the standard linear solid model in viscoelasticity, Calcolo 54 (2) (2017) 587–607.
[8] G.N. Gatica, A. Márquez, S. Meddahi, A mixed finite element method with reduced symmetry for the standard model in linear viscoelasticity, Calcolo 58 (1) (2021) 27, Paper No. 11.
[9] A. Márquez, S. Meddahi, Mixed-hybrid and mixed-discontinuous Galerkin methods for linear dynamical elastic-viscoelastic composite structures, J. Numer. Math. 30 (1) (2022) 43–62.
[10] S. Meddahi, R. Ruiz-Baier, A mixed discontinuous Galerkin method for a linear viscoelasticity problem with strongly imposed symmetry, SIAM J. Sci. Comput. 45 (2023) B27–B56.
[11] D. Boffi, F. Brezzi, M. Fortin, Mixed Finite Element Methods and Applications, in: Springer Series in Computational Mathematics, vol. 44, Springer, Heidelberg, 2013.
[12] D.N. Arnold, G. Awanou, R. Winther, Finite elements for symmetric tensors in three dimensions, Math. Comp. 77 (263) (2008) 1229–1251.
[13] J. Hu, Finite element approximations of symmetric tensors on simplicial grids in Rn: the higher order case, J. Comput. Math. 33 (3) (2015) 283–296.
[14] D.N. Arnold, R.S. Falk, R. Winther, Mixed finite element methods for linear elasticity with weakly imposed symmetry, Math. Comp. 76 (260) (2007) 1699–1723.
[15] D.N. Arnold, G. Awanou, R. Winther, Nonconforming tetrahedral mixed finite elements for elasticity, Math. Models Methods Appl. Sci. 24 (4) (2014) 783–796.
[16] J. Gopalakrishnan, J. Guzmán, Symmetric nonconforming mixed finite elements for linear elasticity, SIAM J. Numer. Anal. 49 (4) (2011) 1504–1520.
[17] S. Wu, S. Gong, J. Xu, Interior penalty mixed finite element methods of any order in any dimension for linear elasticity with strongly symmetric stress tensor, Math. Models Methods Appl. Sci. 27 (14) (2017) 2711–2743.
[18] S. Du, HDG methods for Stokes equation based on strong symmetric stress formulations, J. Sci. Comput. 85 (2020) 19, Paper No. 8.
[19] W. Qiu, J. Shen, Jiguang, K. Shi, An HDG method for linear elasticity with strong symmetric stresses, Math. Comp. 87 (2018) 69–93.
[20] B. Cockburn, J. Gopalakrishnan, R. Lazarov, Unified hybridization of dis- continuous Galerkin, mixed, and continuous Galerkin methods for second order elliptic problems, SIAM J. Numer. Anal. 47 (2009) 1319–1365.
[21] S. Du, F.-J. Sayas, An Invitation to the Theory of the Hybridizable Discontinuous Galerkin Method, in: Springer Briefs in Mathematics, 2019.
[22] N.C. Nguyen, J. Peraire, B. Cockburn, High-order implicit hybridizable discontinuous Galerkin methods for acoustics and elastodynamics, J. Comput. Phys. 230 (12011) 3695–3718.
[23] S.-C. Soon, B. Cockburn, H.K. Stolarski, A hybridizable discontinuous Galerkin method for linear elasticity, Internat. J. Numer. Methods Engrg. 80 (2009) 1058–1092.
[24] B. Cockburn, G. Fu, Devising superconvergent HDG methods with symmetric approximate stresses for linear elasticity by M-decompositions, IMA J. Numer. Anal. 38 (2018) 566–604.
[25] S. Du, F.-J. Sayas, New analytical tools for HDG in elasticity, with applications to elastodynamics, Math. Comp. 89 (2020) 1745–1782.
[26] B. Cockburn, Static Condensation, Hybridization, and the Devising of the HDG Methods, in Building Bridges: Connections and Challenges in Modern Approaches to Numerical Partial Differential Equations, Springer, 2016, pp. 129–177.
[27] M.S. Fabien, M.G. Knepley, R.T. Mills, B. Riviere, Manycore parallel computing for a hybridizable discontinuous Galerkin nested multigrid method, SIAM J. Sci. Comput. 41 (2019) C73–C96.
[28] A. Samii, C. Michoski, C. Dawson, A parallel and adaptive hybridized discontinuous Galerkin method for anisotropic nonhomogeneous diffusion, Comput. Methods Appl. Mech. Engrg. 304 (2016) 118–139.
[29] C. García, G.N. Gatica, S. Meddahi, A new mixed finite element method for elastodynamics with weak symmetry, J. Sci. Comput. 72 (3) (2017) 1049–1079.
[30] R.E. Ewing, J. Wang, Y. Yang, A stabilized discontinuous finite element method for elliptic problems, Numer. Linear Algebra Appl. 10 (2003) 83–104.
[31] R. Dautray, J.L. Lions, Mathematical Analysis and Numerical Methods for Science and Technology: Vol. 5, Evolution Problems I, Springer, Berlin, 2000.
[32] A. Kroó, On Bernstein-Markov-type inequalities for multivariate polynomials in L_q-norm, J. Approx. Theory 159 (2009) 85–96.
[33] C. Schwab, *p*- and *hp*-Finite Element Methods: Theory and Applications in Solid and Fluid Mechanics, Oxford University Press, 1998.
[34] I. Babuška, M. Suri, The *h*-*p* version of the finite element method with quasi-uniform meshes, RAIRO Modél. Math. Anal. Numér. 21 (1987) 199–238.
[35] J.M. Melenk, T. Wurzer, On the stability of the boundary trace of the polynomial L2-projection on triangles and tetrahedra, Comput. Math. Appl. 67 (2014) 944–965.
[36] P. Houston, C. Schwab, E. Süli, Discontinuous *hp*-finite element methods for advection-diffusion-reaction problems, SIAM J. Numer. Anal. 39 (2002) 2133–2163.
[37] I. Perugia, D. Schotzau, An *hp*-analysis of the local discontinuous Galerkin method for diffusion problems, J. Sci. Comput. 17 (2002) 561–571.
[38] Netgen/NGSolve, Finite element library. https://ngsolve.org.